PCHEM 3493

LSU Chemistry ~~2002~~ Safety Agreement

Anytime I am working in or visiting the laboratory, I will follow the laboratory safety practices recommended in the safety lecture and take the following precautions:

1. Wear splash-proof goggles at all times.
2. Know the exact location and operation of all safety Equipment!
3. Use reagents and chemicals correctly (Handle acids and toxic chemicals with caution). Know location of MSDS for chemicals used in the laboratory.
4. Do only the experiment assigned by my laboratory instructor. Never work alone in the laboratory!
5. Wear proper lab clothing (lab aprons, gloves, etc.) to provide the maximum possible protection against chemical splash.
6. Place personal belongings: such as purses, backpacks, coats in the designated laboratory areas.
7. Never eat, drink, smoke, dip, or apply lipstick in the chemical laboratory.
8. Dispose of chemical waste materials according to directions of my lab instructor.
9. Help keep the laboratory clean at all times.
10. Use a fume hood when directed to do so.
11. Use good judgment and care when working in the laboratory.
12. Avoid touching hot objects.
13. Read the labels on reagent bottles and containers to make certain that they contain appropriate chemicals for the experiment.
14. Immediately wash chemical splashes on skin\clothes. Wash hands thoroughly before leaving the lab.
15. Immediately report all physical and chemical injuries to lab instructor, no matter how minor it seems.
16. Consult instructor if I'm unsure or feel that a protocol is unsafe. I have the right and obligation to stop any procedure that I feel is unsafe. Be observant and helpful to fellow students in lab emergencies.
17. Orderly, exit lab if fire alarm sounds

I have carefully read and discussed the recommended laboratory safety practices and the precautions listed above. I understand their importance in preserving the safety of everyone in the laboratory. I recognize my responsibility to follow these practices and precautions while I am present in the laboratory.

_____ student's name (print)

_____ student ID#

_____ student's signature

_____ date

_____ course & section

_____ room number

_____ laboratory instructor's signature

_____ date

that students need to learn. The following explanation of the scientific report serves as a generic assignment for the sciences.

The Formal Scientific Research Report

A formal scientific research report is a piece of professional writing addressed to other professionals who are interested in the investigation you conducted. They will want to know why you did the investigation, how you did it, what you found out, and whether your findings were significant and useful. Research reports usually follow a standard five-part format: (1) introduction, (2) methods, (3) results, (4) discussion of results, and (5) conclusions and recommendations.

Introduction. Here you explain briefly the purpose of your investigation. What problem did you address? Why did you address it? You will need to provide enough background to enable the reader to understand the problem being investigated. Sometimes the introduction also includes a "literature review" summarizing previous research addressing the same or a related problem. In many scientific disciplines, it is also conventional to present a hypothesis—a tentative "answer" to the question that your investigation will confirm or disconfirm.

Methods. This is a "cookbook" section detailing how you did your investigation. It provides enough details so that other researchers could replicate your investigation. Usually, this section includes the following subsections: (a) research design, (b) apparatus and materials, and (c) procedures followed.

Results. This section, sometimes headed "Findings," presents the empirical results of your investigation. Often, your findings are displayed in figures, tables, graphs, or charts that are referenced in the text. Even though the data are displayed in visuals, the text itself should also describe the most significant data. (Imagine that the figures are displayed on a view graph and that you are explaining them orally, using a pointer. Your written text should transcribe what you would say orally.) Your figures and tables must have sufficient information to stand alone, including accurate titles and clear labels for all meaning-carrying features.

Discussion of results. This is the main part of the report, the part that will be read with the most care by other professionals. Here you explain the significance of your findings by relating what you discovered to the problem you set out to investigate in your introduction. Did your investigation accomplish your purpose? Did it answer your questions? Did it confirm or disconfirm your hypothesis? Are your results useful? Why or why not? Did you discover information that you hadn't anticipated? Was your research design appropriate? Did your investigation raise new questions? Are there implications from your results that need to be explored? The key to success in this section is to link your findings to the questions and problems raised in the introduction.

Conclusions and recommendations. In this last section, you focus on the main things you learned from the investigation and, in some cases, on the practical applications of your investigation. If your investigation was a pure research project, this section can be a summary of your most important findings along with recommendations for further research. If your investigation was aimed at making a practical decision (for example, an engineering design decision), here you recommend appropriate actions. What you say in this section depends on the context of your investigation and the expectations of your readers.

Redox Titration of Ferricyanide to Ferrocyanide with Ascorbic Acid: Illustrating the Nernst Equation and Beer–Lambert Law

Tina H. Huang,* Gail Salter, Sarah L. Kahn, and Yvonne M. Gindt
Department of Chemistry, Lafayette College, Easton, PA 18042; *huangt@lafayette.edu

Electrochemistry and the Nernst equation are introduced in the chemistry curriculum at this college during second semester of general chemistry. The electrochemical concepts and applications are discussed further in analytical chemistry, physical chemistry, and biochemistry courses. Considering the prevalence of electrochemical concepts in many areas of chemistry, we feel that it is important that the students understand the fundamental electrochemical concepts early in the chemistry curriculum through hands-on experimentation. In the past, we had problems integrating an experiment that explained the Nernst equation well. For the last two years, we have incorporated a redox titration of ferricyanide ion, $[Fe(CN)_6]^{3-}$, to ferrocyanide ion, $[Fe(CN)_6]^{4-}$, to show the students how the reduction potential of a redox couple is affected by the concentrations of the redox species, and how they can use the Nernst equation to calculate the standard reduction potential of a half-reaction. While others have reported laboratory experiments dealing with the Nernst equation in this *Journal (1–4)*, these are usually written for more advanced courses such as physical chemistry and instrumental analysis and require techniques (i.e., cyclic voltammetry) that are often beyond the knowledge of typical first-year undergraduate students. In the experiment described here, our students obtain excellent data and we have encountered few problems with this laboratory.

The reduction of ferricyanide ion [or hexacyanoferrate(III)] to ferrocyanide [hexacyanoferrate(II)] coupled with the oxidation of ascorbic acid ($C_6H_8O_6$) to dehydroascorbic acid ($C_6H_6O_6$) was studied by Mehrotra, Agrawal, and Mushran *(5)*:

$$\underset{\text{(yellow)}}{\text{ferricyanide}} + e^- \longrightarrow \underset{\text{(colorless)}}{\text{ferrocyanide}} \qquad (1)$$

$$\underset{\text{(colorless)}}{\text{ascorbic acid}} \longrightarrow \underset{\text{(colorless)}}{\text{dehydroascorbic acid}} + 2H^+ + 2e^- \qquad (2)$$

We chose the ferricyanide/ferrocyanide redox system for this experiment because it is well-characterized *(5–9)*, and the concentration of ferricyanide can be easily monitored using UV–vis spectroscopy. We tried several other redox couples, but we found this system to be superior owing to its rapid equilibration time along with its relative inertness towards atmospheric oxygen.

In our general chemistry curriculum, the students are introduced to the concepts of electrochemistry and cell potential using the Nernst equation. While the students will be familiar with the expression given for the overall reaction, the expression using only the reduction of a species will be a new concept that must be introduced in the laboratory. For example, a generic reduction half-reaction, eq 3, and its corresponding Nernst expression, eq 4, are

$$A + ne^- \longrightarrow B \qquad (3)$$

$$E = E^\circ - \frac{RT}{nF}\ln\frac{[B]}{[A]} \qquad (4)$$

In eq 3, A is being reduced to B with the addition of n electrons. E° is the standard reduction potential of the A/B couple (one parameter that the students will find), while E is the reduction potential that the students monitor during the course of the titration for the specific conditions of [B] and [A]. The students will also find n, the number of electrons transferred during the reduction.

For the reduction of ferricyanide to ferrocyanide, we can write the Nernst expression as

$$E = E^\circ - \frac{RT}{nF}\ln\frac{[\text{ferro}]}{[\text{ferri}]} \qquad (5)$$

where ferro and ferri are abbreviated forms of ferrocyanide and ferricyanide, respectively. Starting with only ferricyanide present in solution, small aliquots of ascorbic acid are added to the solution. After each aliquot, both the concentration of ferricyanide and the solution potential, E, are measured using UV–vis spectroscopy and a two-electrode potentiometric setup, respectively. The plot of the solution potential versus ln([ferro]/[ferri]) gives a line whose y intercept is the standard reduction potential of the ferrocyanide/ferricyanide couple. The number of electrons involved in the reduction of the couple, n, is easily calculated from the slope of the line. The ascorbic acid is used solely as the reductant in the reaction; we do not find the reduction potential of the ascorbic acid/dehydroascorbic acid couple.

The experiment provides an excellent illustration of the relationship between the concentration of species in a redox couple and the potential of the species. The students are exposed to a practical method of measuring a redox couple potential using spectroelectrochemistry.

Experimental Section

Reagents

Potassium hexacyanoferrate, $K_3Fe(CN)_6$, ascorbic acid, and potassium dihydrogen phosphate are purchased from Sigma-Aldrich (St. Louis, MO). All solutions are prepared using deionized water.

Instrumentation

The electrical potential, E, of the solution is monitored using a simple apparatus that had a platinum wire as working electrode, a saturated silver–silver chloride (Ag/AgCl) electrode as the reference electrode, and a digital voltmeter to monitor the difference in potential between the two electrodes. We also used either a Beckman Spec-20 (Sequoia Turner model 340) or an Ocean Optics (Chem 2000) UV–vis spectrophotometer to monitor the absorbance of the ferricyanide species in the solution.

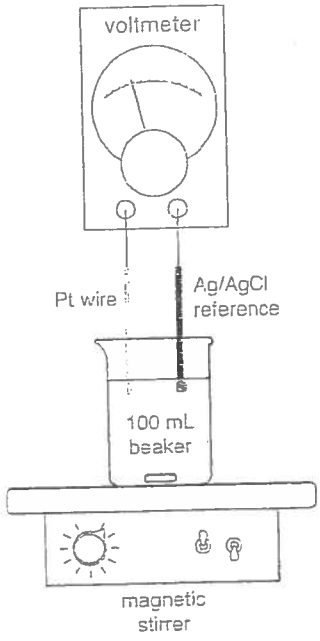

Figure 1. Experimental setup required for redox titration. The apparatus consists of a single Pt wire as the working electrode, a Ag/AgCl electrode as the reference electrode, and a voltmeter to monitor the potential of the Pt wire relative to the Ag/AgCl reference electrode.

Experimental Procedure

Two stock solutions, 0.50 mM $K_3Fe(CN)_6$ solution in 0.10 M pH 7 phosphate buffer and a 0.060 M ascorbic acid, are prepared by the instructor prior to the experiment. Approximately 30 mL of the ferricyanide solution and 1 mL of ascorbic solution are required by each group of students. The students start by immersing their platinum working electrode and the Ag/AgCl reference electrode in approximately 30 mL of 0.500 mM $K_3Fe(CN)_6$ solution (Figure 1). The solution is stirred constantly via magnetic stirring with special care taken to ensure the stir bar does not hit either electrode. Once the electrodes are set up properly and a stable voltage reading is obtained, a small portion of the bright yellow solution is removed to measure the absorbance of the ferricyanide at 420 nm. The solution is transferred back to the beaker after a successful absorbance reading. This absorbance is used to calculate the initial concentration of ferricyanide.

The students are now ready to begin their titration. A small aliquot, 5 μL, of 0.060 M ascorbic acid is added to the beaker with the electrodes. We generally use micropipets for the titration; it is critical to use small volumes of the titrant since we are making the approximation that the total volume of the solution is unchanged over the course of the experiment. We found that a 5 μL aliquot of titrant is optimal for the concentrations of solutions used; the students generally measure 15–20 samples over the course of the titration. Smaller volumes increase the length of the experiment while larger volumes decrease the number of data points used in the analysis.

After the ascorbic acid is added, the solution is allowed to equilibrate for two minutes. After two minutes, the potential and the absorbance at 420 nm are obtained; both readings should decrease over the course of the titration. Another aliquot of titrant is added at this point, and the entire process is repeated until the solution appears to be colorless.

Data Analysis

Our students analyze their data using the Excel spreadsheet. The calculations could also be done via a calculator. Using the Beer–Lambert law,

$$A = \varepsilon b c \tag{6}$$

the concentration, c, of ferricyanide is calculated from the absorbance of the solution. The molar absorptivity, ε, of the ion is 1.02×10^3 L mol^{-1} cm^{-1} and the path length, b, of 1 cm is used. The quantity of ferrocyanide is found from the quantity of ferricyanide lost during the titration, assuming no side reactions occur

$$[\text{ferri}]_{\text{initial}} = [\text{ferro}]_x + [\text{ferri}]_x \tag{7}$$

Table 1. Experimental Data Collected by One Group of Students

A	[ferri]/ (10^{-4} mol L^{-1})	[ferro]/ (10^{-4} mol L^{-1})	[ferro]/[ferri]	ln([ferro]/[ferri])	Potential/ mV
0.588	5.76	—	—	—	—
0.564	5.53	0.24	0.0433	-3.14	308.8
0.539	5.28	0.47	0.0890	-2.42	289.7
0.515	5.05	0.71	0.141	-1.96	277.9
0.493	4.83	0.93	0.193	-1.65	269.1
0.473	4.64	1.12	0.241	-1.42	261.6
0.445	4.36	1.40	0.321	-1.14	255.2
0.397	3.89	1.87	0.481	-0.732	244.7
0.373	3.66	2.10	0.574	-0.555	239.8
0.342	3.35	2.41	0.719	-0.330	233.6
0.297	2.91	2.85	0.979	-0.0212	225.6
0.273	2.68	3.08	1.15	0.140	221.2
0.248	2.43	3.33	1.37	0.315	216.7
0.211	2.07	3.69	1.78	0.577	209.9
0.162	1.59	4.17	2.62	0.963	200
0.143	1.40	4.36	3.11	1.13	195.6

where the subscript x indicates the [ferro] and [ferri] after the subsequent addition of ascorbic acid during the titration. The ln([ferro]/[ferri]) is calculated for each data point. To reduce problems owing to poor signal-to-noise at low concentrations of either species, data points outside the range of -1 to +1 for the ln([ferro]/[ferri]) are discarded from further analysis. The solution potential, E, is plotted versus ln([ferro]/[ferri]). The data are fit to a line using least-squares analysis. The y intercept is E°, the standard reduction potential of the ferrocyanide/ferricyanide couple versus the Ag/AgCl standard, and the negative slope of the line is RT/nF. Our students are able to solve the slope for n, given the constants and the temperature.

Hazards

There are no significant hazards associated with this experiment. The $[Fe(CN)_6]^{4-}$ and $[Fe(CN)_6]^{3-}$ are stable complex ions under the conditions of the experiment. The material data safety sheets for the complex ions do recommend the avoidance of strong acids and high temperature, which could cause the complex ion to decompose with the formation of hydrogen cyanide, a toxic gas. Also, both complex ions are toxic via ingestion.

Results

Typical data recorded during the course of the experiment for one group of students are shown in Table 1, while the data plotted as described above are shown in Figure 2. The average intercept value with the standard deviation is 0.228 ± 0.012 V and 0.224 ± 0.006 V for two different semesters. The standard reduction potential can be converted to the SHE standard by adding 0.197 V to the potential obtained with the Ag/AgCl standard (the value for the saturated Ag/AgCl electrode). The standard reduction potentials at pH 7 calculated by the students over the last two semesters (0.425 V and 0.421 V) agree well with the reported value of 0.430 V *(10)*. The number of electrons, n, calculated for the two different semesters are 1.04 ± 0.24 and 0.97 ± 0.05, respectively.

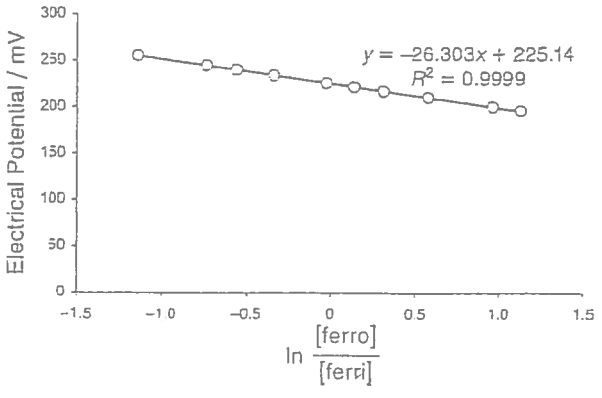

Figure 2. A plot of potential vs ln([ferro]/[ferri]) using the data in Table 1 (using potential range of 255.2–195.6 mV). The linear regression line is calculated using the trendline function in Microsoft Excel.

Conclusions

The redox titration of ferricyanide to ferrocyanide using ascorbic acid as the titrant is an effective method to illustrate the Nernst equation. The students can visually see the effect of the concentration term [ferro]/[ferri] in the Nernst equation on the potential measured. This laboratory also offers several additional benefits: The students use more advanced instrumentation and specialized equipment (i.e., reference electrodes, micropipetters) at the beginning of their chemistry curriculum. Also, they learn the process of using experimental data to calculate the standard reduction potential and number of electrons for the reduction half-reaction of ferricyanide to ferrocyanide. The laboratory forces the student to graphically interpret the Nernst equation.

A student survey was done at the end of the experiment: 80% of the students surveyed said they learned something new in the lab, and 82% said they would recommend that this lab be used in the future. Also, we have found the laboratory to have good reproducibility with outstanding results. It provides an excellent illustration of the Nernst equation for the experimental laboratory.

Acknowledgments

The authors wish to acknowledge Michael Chejlava for his technical assistance. This work was supported by the Department of Chemistry at Lafayette College.

Supplemental Material

Instructions for the students including a report form and notes for the instructor are available in this issue of *JCE Online*.

Literature Cited

1. Walczak, M. M.; Dryer, D. A.; Jacobson, D. D.; Foss, M. G.; Flynn, N. T. *J. Chem. Educ.* 1997, *74*, 1195–1197.
2. DeAngelis, T. P.; Heineman, W. R. *J. Chem. Educ.* 1976, *53*, 594–597.
3. Arévalo, A.; Pastor, G. *J. Chem. Educ.* 1985, *62*, 882–884.
4. Thompson, M. L.; Kateley, L. J. *J. Chem. Educ.* 1999, *76*, 95–96.
5. Mehrotra, U. S.; Agrawal, M. C.; Mushran, S. *J. Phys. Chem.* 1969, *73*, 1996–1999.
6. Kolthoff, I. M.; Tomsicek W. J. *J. Phys. Chem.* 1935, *39*, 945–954.
7. Blaedel, W. J.; Engstrom, R. C. *Anal. Chem.* 1978, *50*, 476–479.
8. Watkins, K. W.; Olson, J. A. *J. Chem. Educ.* 1980, *57*, 157–158.
9. Zahl, A.; van Eldik, R.; Swaddle, T. W. *Inorg. Chem.* 2002, *41*, 757–764.
10. Dutton, P. L. *Methods in Enzymology* 1978, *7*, 411–435.

AN 014.S20

MEASUREMENT OF THE REDUCTION OF POTASSIUM FERRICYANIDE BY L-ASCORBIC ACID WITH A SHIMADZU UV-1700 SPECTROPHOTOMETER USING A STOPPED-FLOW ACCESSORY.

The reduction of Potassium Ferricyanide by Ascorbic Acid is a well known kinetic reaction that was first published by Tonomura *et al.*[1] The speed of this reaction is dependent on the pH value of the solution which makes this reaction a very useful one for testing the performance of kinetic instruments

Keywords: Stopped-Flow Accessory, Shimadzu UV-1700, Rapid Kinetics

Introduction

When Potassium Ferricyanide ($K_3Fe(CN)_6$) is dissolved and brought into solution with L-Ascorbic Acid (Vitamin C, $C_6H_8O_6$), the Ferricyanide ($Fe(CN)_6^{3-}$) can be reduced by the Ascorbic Acid (AA) to form $Fe(CN)_6^{4-}$. Being an acid AA is present in the solution in the form of AA, AA^- and AA^{2-}, the ratio of these depending on the pH of the solution

$$AA \leftrightarrow AA^- + H^+$$

$$AA^- \leftrightarrow AA^{2-} + 2H^+$$

This also means that the speed of the reaction is determined by the pH of the solution. Two of the forms in which AA is present in the solution, AA^- and AA^{2-}, can react with Ferricyanide

Methodology

The reaction mechanisms for the reduction of Ferricyanide by Ascorbic Acid are

$$AA^- + Fe(CN)_6^{3-} \xrightarrow{k_1} AA^{\cdot} + Fe(CN)_6^{4-}$$

and

$$AA^{\cdot} + Fe(CN)_6^{3-} \xrightarrow{k_2} AA^{\circ} + Fe(CN)_6^{4-} + H^+$$

for the AA^- form and

$$AA^{2-} + Fe(CN)_6^{3-} \xrightarrow{k_3} AA^{-\cdot} + Fe(CN)_6^{4-}$$

and

$$AA^{-\cdot} + Fe(CN)_6^{3-} \xrightarrow{k_4} AA^{\circ} + Fe(CN)_6^{4-}$$

for the AA^{2-} form. In these equations AA° is the oxidised form of AA, $C_6H_6O_6$.

The free radicals formed in this reaction instantaneously react with $Fe(CN)_6^{3-}$ and only k_2 and k_4 contribute to the pseudo first order rate constant k, which can be used if $[AA] >> [Fe(CN)_6^{3-}]$. The concentration of $Fe(CN)_6^{3-}$ during the reaction is then given by

$$[Fe(CN)_6^{3-}] = [Fe(CN)_6^{3-}]_0 \cdot \exp^{-kt}$$

Experimental

Potassium Ferricyanide has an absorbance maximum at 420 nm, this can be seen in the spectrum of $K_3Fe(CN)_6$ shown in Figure 1.

All kinetic traces were collected at this wavelength with an AA syringe solution concentration of 20 mM and a $Fe(CN)_6^{3-}$

concentration of 1 mM in the syringes. The experiments were performed at room temperature and the pH value was determined by the Ascorbic Acid concentration (pH ≈ 3).

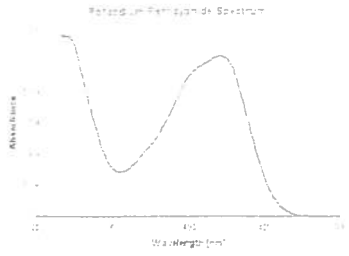

Figure 1: Spectrum of $K_3Fe(CN)_6$

First the acquisition process was started on the Shimadzu UV-1700 spectrophotometer and subsequently the syringes on the SFA-20 were pushed by hand to start the reaction in the cell between Ferricyanide and Ascorbic Acid. The SFA-20 stopped-flow accessory used for these measurements with the Shimadzu UV-1700 was equipped with a standard cell. Kinetic traces were collected for 10 seconds with a time resolution of 100 ms per data point and 101 data points in total were recorded for every trace.

Results

Traces of 14 separate experimental shots were recorded with very good reproducibility. This can be seen in Figure 2 where all the individual traces are shown for the first 3.5 seconds only, because the reaction was over after 3-4 seconds.

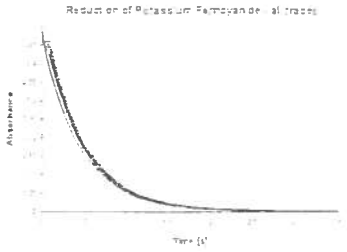

Figure 2: All kinetic traces collected for the reduction of $K_3Fe(CN)_6$

A single trace was then used to fit first order reaction kinetics. Both the original data and the fit to the data are shown in Figure 3.

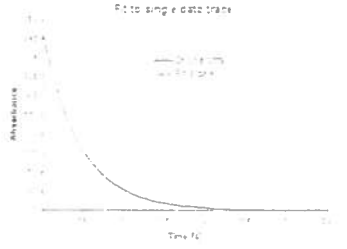

Figure 3: Kinetic trace for $K_3Fe(CN)_6$ reduction with a fit to the data

The first order rate constant found for the reaction was k = 2.15 s^{-1}, which is in good agreement with the value found in the literature[1].

Conclusion

The first order kinetics assumption provides a very good fit to the original data, proving that it was safe to make this assumption with the used concentrations of reagents. Also, the quality of the data collected with the Shimadzu UV-1700 spectrophotometer was very good and consistent. These experiments therefore prove that the Shimadzu UV-1700 is a very suitable spectrophotometer to measure fast kinetic reactions reliably in conjunction with the SFA-20 stopped-flow accessory.

References

[1] B. Tonomura *et al*., Analytical Biochemistry 84 (1978) 370-383

Acknowledgements

We would like to thank Shimadzu U.K. for making the UV-1700 available to us for measurements

Hi-Tech Scientific contacts:

General Manager: Victor Higgs

Technical Manager: Ted King

Sales Office Manager: David Mitchell

Technical Sales Engineer: Melanie Nijman

HI-TECH SCIENTIFIC

Hi-Tech Scientific, Brunel Road, Salisbury SP2 7PU. United Kingdom

Telephone: National 01722 432320

International +44 1722 432320 USA Toll Free 1 800 334 0724

Facsimile: National 01722 432324 International +44 1722 432324

State	T_e	ω_e	$\omega_e x_e$	B_e	α_e	D_e (10^{-4} cm^{-1})	r_e (Å)	Observed Transitions: Design.	Observed Transitions: ν_{00}	References
										DEC 1976 A
$^1H^{35}Cl$		μ = 0.97959272			D_0^0 = 4.433$_6$ eV[a]		I.P. = 12.74$_8$ eV[b]		200-210 eV	(50)(60)
		Rydberg series corresponding to excitation of a 2p electron.								(55)
		Numerous absorption bands above 123000 cm^{-1}, tentatively assigned to higher members of the Rydberg series starting with L and M and converging to A $^2\Sigma^+$ of HCl$^+$.								(55)
M ($^1\Sigma^+$) (117811)		[1529]	v=0...5 observed. Assigned as $3p\sigma\,3p\pi^4\,5s\sigma$.[c]					M← X,	117093	(55)*
L ($^1\Sigma^+$, $^1\Pi$) 111280		1531	52		Assigned as $3p\sigma\,3p\pi^4\,4p\sigma/\pi$.[c]			L← X,	110555	(55)*
		Many other absorption bands in the region 83000 - 93000 cm^{-1} corresponding to Rydberg states strongly perturbed by the V $^1\Sigma^+$ state which itself gives rise to many perturbed bands.								(62)
K $^1\Pi$ (89861)		[2604.6]	Z		[9.230][d]		[-12.$_6$][d]	[1.3654]	K← X, R 89680.5 Z	(62)
H $^1\Sigma^+$ (89120)		[2093.8]	Z		[8.4410]		[8.93]	[1.4278]	H← X, R 88684.5 Z	(62)
E $^1\Sigma^+$ (84193)		[2138.6]	Z		[6.6423]		[36.2]	[1.6096]	E← X, R 83780.2 Z	(62)
g $(^3\Sigma^-)1$	e [84329.7]				[10.36][f]		[17][f]	[1.28$_9$]	g← X, 82847.4 Z	(48)*
f_1 $^3\Delta_1$	e [84006.1]				[10.27$_0$][g]		[-13][g]	[1.294]	f_1← X, 82523.8 Z	(48)*
D $^1\Pi$	h [83972.0]				[9.79$_4$][i]		[20.$_5$][i]	[1.326]	D← X, R 82489.7 Z	(48)*
d_0 $^3\Pi_0$	h [83753.6]				[9.40$_4$][j]		[-2.$_2$][j]	[1.353]	d_0← X, R 82271.3 Z	(48)*
f_2 $^3\Delta_2$	e [83497.7]				[10.85$_1$][k]		[29.$_5$][k]	[1.259]	f_2← X, V 82015.4 Z	(48)*
f_3 $^3\Delta_3$	e [83308.2]				[9.45][g]		[-1.$_3$][g]	[1.34$_9$]	f_3← X, R 81825.9 Z	(48)*
d_1 $^3\Pi_1$	h [83255.6]				[9.76$_8$][l]		[8][l]	[1.327]	d_1← X, R 81773.3 Z	(48)*
d_2 $^3\Pi_2$	h [83083.0]				[8.63$_2$][m]		[-14][m]	[1.412]	d_2← X, R 81600.7 Z	(48)*
C $^1\Pi$	n 77575	[2684.0]	Z o		[9.33$_3$]	o		[1.358]	C← X,[p] R 77485.3 Z	(1)* (44)
V $^1\Sigma^+$	q 77293.$_0$	877.16	Z 16.04[r]		2.727	-0.026	1.02[r]	2.512	V↔X,[s] R 76245.3 Z	(8)(9)(48)*
		Continuous emission spectrum with maximum at 38900 cm^{-1}.							V→A	(9)

State	T_e	ω_e	$\omega_e x_e$	B_e	α_e	D_e (10^{-4} cm^{-1})	r_e (Å)	Observed Transitions: Design.	Observed Transitions: ν_{00}	References

State	T_e	ω_e	$\omega_e x_e$	B_e	α_e	D_e (10^{-4} cm^{-1})	r_e (Å)	Observed Transitions: Design.	Observed Transitions: ν_{00}	References
$^1H^{35}Cl$ (continued)										
X $^1\Sigma^+$	0	2990.946_3[x]	52.8186[y]	10.59341_6[xz]	0.30718_1[a']	5.3194[zb']	1.27455_2[c']	Rot.-vibr. bands[d'e']		(19)(28)
								Rotation spectrum[f'e']		(4)(23)(52)
								Raman cross sections		(58)
								Mol. beam electric[g'] and magnetic[h'] reson.		(41)(64) (37)

$^1H^{35}Cl$ (continued):

[x] Applying the Dunham corrections (28) obtain ω_e = 2991.0904 and B_e = 10.593553. Additional corrections (adiabatic, non-adiabatic) discussed by (49). Vibrational levels up to v=5 have been observed in infrared absorption (12)(19)(28) and emission (10), higher levels in the V→X bands (8)(9). Dunham potential coefficients (61). Most recent ab initio values of the ground state molecular constants (59); charge distribution (40).

[y] $\omega_e y_e = +\ 0.2243_7$, $\omega_e z_e = -\ 0.0121_8$ (28).

[z] Slightly different constants in (11)(26)(31). These papers and (39) give also constants for $H^{37}Cl$.

[a'] $+ 0.001772_4(v+\frac{1}{2})^2 - 0.0001201(v+\frac{1}{2})^3$.

[b'] $-7.51_0 \times 10^{-6}(v+\frac{1}{2}) + 4.0_0 \times 10^{-7}(v+\frac{1}{2})^2$; higher order terms in (28). See also (30).

[c'] Uncorrected value from the $B_e(\equiv Y_{01})$ given in the table. The internuclear distance at the minimum of the Born-Oppenheimer curve is r_e = 1.2746149 Å (49)(63).

[d'] Absolute intensities ($cm^{-2}atm^{-1}$) of the

1-0 band:	130	(5)
2-0 band:	2.9	(5)
	3.70	(17)(45)
3-0 band:	0.023	(5)

[e'] Pressure-induced shifts (by foreign gases) of rotation-vibration and rotation lines (13)(14)(21)(22)(24). For discussions of pressure-induced bands and pure rotation lines (ΔJ=2) see (32)(36). Self and foreign-gas line broadening (5)(7)(16)(17)(18)(29)(43)(45)(47)(52). Infrared absorption in liquid and solid phases (42)(51).

[f'] Absolute intensity measurements (25)(34).

[g'] $\mu_{e\ell}(v=0,1,2)$ = 1.1085, 1.1390, 1.1685 D, resp. (41). Dipole moment function (41)(54); see also (53)(56). g_J = 0.4594, also quadrupole and other hyperfine coupling constants (41)(64); see also (35)(53).

[h'] Proton spin - rotation interaction constant (15)(37).

State	T_e	ω_e	$\omega_e x_e$	B_e	α_e	D_e (10^{-4} cm^{-1})	r_e (Å)	Observed Transitions: Design.	Observed Transitions: ν_{00}	References
$^2H^{35}Cl$		μ = 1.90441364		D_0^0 = 4.485$_2$ eV[a]		I.P. = 12.75$_6$ eV[b]				DEC 1976 A
		Numerous absorption bands above 123000 cm^{-1}; see ^{1}HCℓ.								(25)
M ($^1\Sigma^+$) (117670)		[1220] v=0...8 observed. } See ^{1}HCℓ.						M ← X,	117214	(25)
L ($^1\Sigma^+$,$^1\Pi$) 111268		1126 37 } See ^{1}HCℓ.						L ← X,	110748	(25)
		Many other absorption bands in the region 83000 - 93000 cm^{-1}; see ^{1}HCℓ.								(27)
K $^1\Pi$	(89945)	[1858.8] Z		[4.9306][c]			[1.3399]	K ← X, R	89708.9 Z	(27)
H $^1\Sigma^+$	(88944)	[1631.8] Z		[4.6578]		[0.14$_7$]	[1.3786]	H ← X, R	88694.0 Z	(27)
E $^1\Sigma^+$	(84417)	[1186.9] Z		[3.2960]		[-2.48]	[1.6388]	E ← X, R	83944.9 Z	(27)
f_1 $^3\Delta_1$	[83626.2]			[5.21$_0$]		[0.96]	[1.303]	f_1 ← X, R	82560.4 Z	(22)
D $^1\Pi$	(82632)	[1918.8] Z		5.14$_2$[d]	0.152	[2.$_0$][d]	1.312	D ← X, R	82525.9 Z	(22)
d_0 $^3\Pi_0$	[83350.3]			[5.01$_6$]		[1.3$_5$]	[1.328]	d_0 ← X, R	82284.5 Z	(22)
f_2 $^3\Delta_2$	[83140.0]			[5.32$_8$]		[3.9]	[1.289]	f_2 ← X, R	82074.2 Z	(22)
d_1 $^3\Pi_1$	[82855.0]			[5.13$_7$][e]		[1.9][e]	[1.313]	d_1 ← X, R	81789.2 Z	(22)
d_2 $^3\Pi_2$	[82695.6]			[4.74$_7$][f]		[-7][f]	[1.366]	d_2 ← X, R	81629.8 Z	(22)
C $^1\Pi$	77558.5	2027.1 Z	34.98[g]	4.962[h]	0.120	[1.16]	1.336	C ← X, R	77497.6 Z	(9)(18)*
b_0 $^3\Pi_0$	[76548.0]			[5.21$_8$]			[1.302]	b_0 ← X, R	75482.2 Z	(18)*
b_1 $^3\Pi_1$	75199.3	2015.4 Z	29.1	[5.10$_0$][i]	0.12$_9$[j]	[3.$_5$]	1.309	b_1 ← X, R	75133.9 Z	(9)(18)*
b_2 $^3\Pi_2$	[75912.7]			[4.90$_5$]			[1.343]	b_2 ← X, R	74846.9 Z	(18)*
X $^1\Sigma^+$	0	2145.163 Z	27.1825[k]	5.448794[l]	0.113291[k]	1.39[m]	1.274581	Rot.-vibr. bands[nop]		(2)(3)(7)(8)
		2090.80 = 2145.163 − 2(27.1825)						Rotation sp.[p]		(1)(5)(21)(23)
								Mol. beam el. reson.[q]		(16)

Vibrations of Carbon Dioxide and Carbon Disulfide

Purpose

Vibration frequencies of CO_2 and CS_2 will be measured by Raman and Infrared spectroscopy. The spectra show effects of normal mode symmetries on gross selection rules. A Fermi resonance in the Raman spectrum will be interpreted in terms of interacting normal modes. Vibration frequencies will be calculated with *ab initio* quantum-chemical methods and compared to experimental frequencies. CS_2 has longer bonds and lower vibration frequencies than CO_2.

Introduction

Linear triatomic molecules such as CO_2 and CS_2 have four vibrational normal modes but just three fundamental vibration frequencies because two modes are degenerate.[1] The stretching mode is totally symmetric so it is inactive in infrared spectra and active in Raman spectra. The

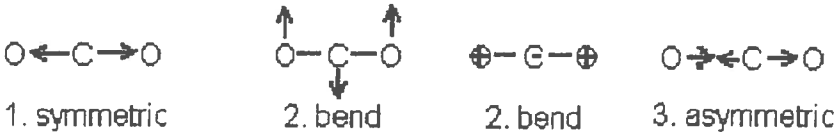

asymmetric stretching vibration and the degenerate bending vibrations are infrared active and Raman inactive. Infrared activities follow from the gross selection rule that "displacements of a normal mode must cause a change in dipole moment in order to be spectroscopically active in the infrared."[1] The CO_2 and CS_2 molecules have a center of symmetry located at the carbon atom. Such molecules obey the exclusion rule, "In a centrosymmetric molecule no Raman-active molecule is also infrared-active and no infrared-active vibration is also Raman active."[2] The symmetric stretching vibration is Raman active and infrared inactive. The bend and asymmetric stretch are infrared active and are, for CO_2, routinely observed in the background scan on an FTIR instrument.[3]

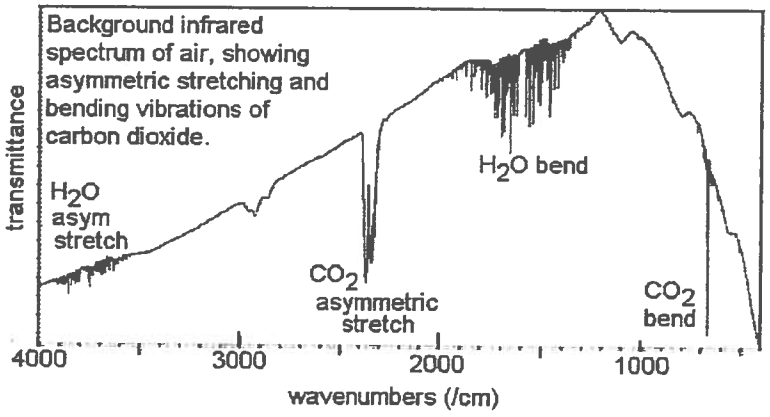

Vibration frequencies will be calculated quantum-mechanically for both CO_2 and CS_2, using three methods: Hartree Fock, Hartree Fock plus second-order Moller-Plesset correction, and density functional theory. Hartree-Fock calculations are the simplest and most robust of the three methods and are good for initial geometry optimization. Vibration frequencies calculated from simple Hartree Fock theory are usually too large by about 10%. Second-order Moller-Plesset

2349

3 2

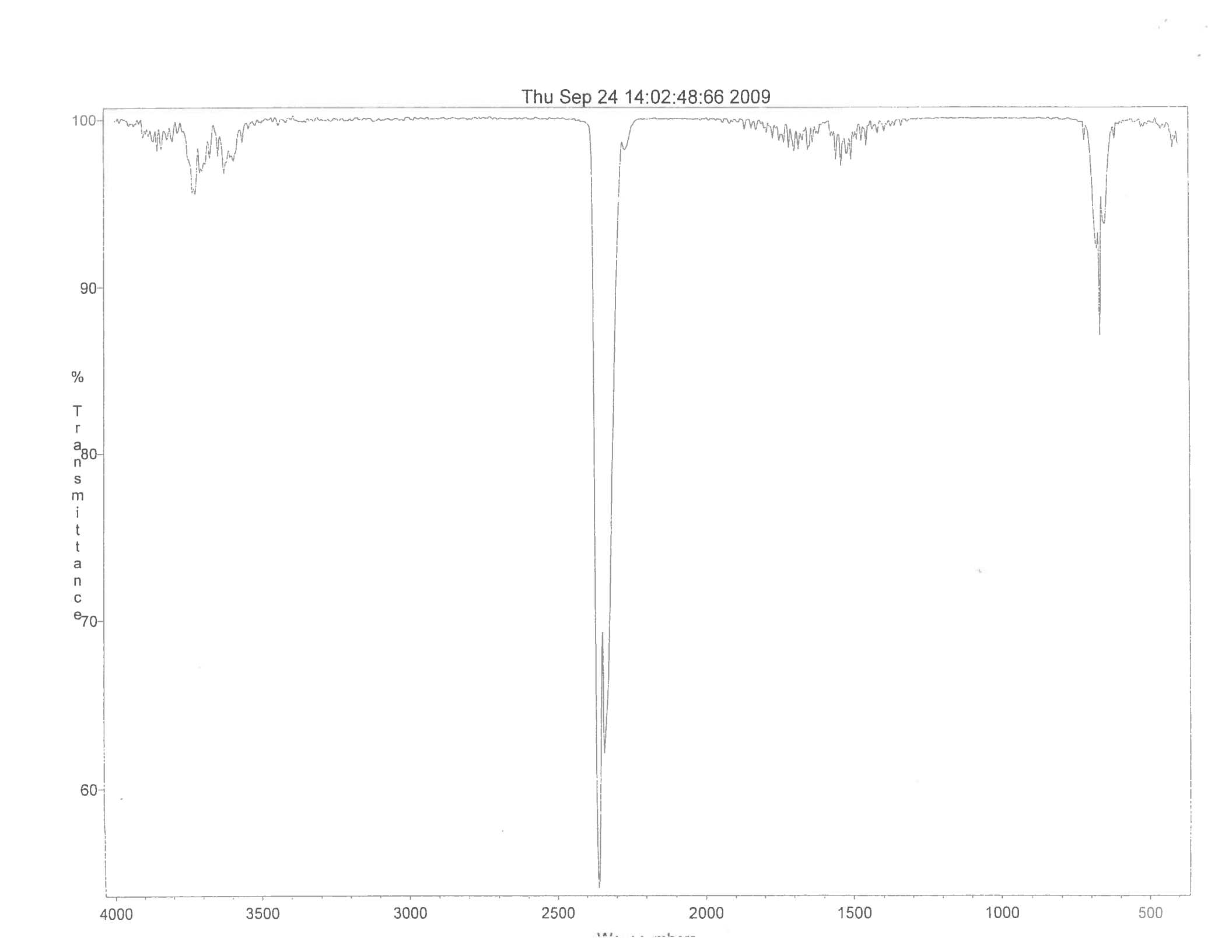
Thu Sep 24 14:02:48:66 2009
100
90
80
70
60
% Transmittance
4000
3500
3000
2500
2000
1500
1000
500

TABLE 64 (*continued*)

State	Point Group	T_0	Vibrational Frequencies ν_1	ν_2	ν_3	Rotational Constants A_0	B_0	C_0	r_0(XY)	r_0(YZ)	α	Electron Configuration	Observed Transitions	References	Remarks
CO_2		I.P. = 13.769 eV; D(O—CO) = 5.453 eV (see energy level diagram Fig. 190)												(80)	
		Three broad continua with maxima at 570, 350 and 280 Å													
		Three Rydberg series: $\nu = 156300 - \begin{cases} R/(n+0.29)^2; & n=3,\ldots,8 \\ R/(n+0.44)^2; & n=3,\ldots,8 \\ R/(n-0.05)^2; & n=4,\ldots,8 \end{cases}$ with first members at 146490, 147280 and 149500 respectively, converging to a new state of CO_2^+ viz. the predicted $^2\Sigma_g^+$												(1189)	
		Two Rydberg series joining on to $\tilde{R}$ and $\tilde{S}$: $\nu = 146800 - \begin{cases} R/(n+0.008+3.25/n^3)^2; & n=3,\ldots,18 \\ R/(n-0.305)^2; & n=3,\ldots,18 \end{cases}$ [a] converging to the $^2\Sigma_u^+$ state of CO_2^+												(1191)	Henning series; see Fig. 189, p. 502
$\tilde{S}$	$D_{\infty h}$	132977	1273										$\tilde{S} \leftarrow \tilde{X}$ 752 Å	(1191)	Sharp bands; repr. (1191)
$\tilde{R}$	$D_{\infty h}$	130774	1275										$\tilde{R} \leftarrow \tilde{X}$ 766 Å	(1191)	Diffuse bands; repr. (1191)
		Rydberg series joining on to $\tilde{L}$: $\nu = 130726 - R/(n - 0.063 - 0.0009/n)^2$; $n = 3,\ldots,10$,												(1191)	Converging to the $^2\Pi_{\frac{1}{2}u}$ state of CO_2^+ [b]
		Rydberg series parallel to above: $\nu = 130034 - R/(n - 0.044 - 0.34/n)^2$; $n = 4,\ldots,9$												(1191)	Converging to the $^2\Pi_{\frac{1}{2}u}$ state of CO_2^+ [b]
$\tilde{M}$		127443	1120										$\tilde{M} \leftarrow \tilde{X}$ 784–758 Å	(1191)	Progression of five members
$\tilde{L}$	$D_{\infty h}$	127065	1127										$\tilde{L} \leftarrow \tilde{X}$ 787–712 Å	(1189) (1191)	Progression of six members; repr. (1191)
		Two weak Rydberg series joining on to $\tilde{E}$ and $\tilde{G}$: $\nu = 111250 - \begin{cases} R/(n-0.67)^2; & n=3,4,\ldots,11 \\ R/(n-0.97)^2; & n=4,5,\ldots,11 \end{cases}$												(1189)	
		Two strong Rydberg series joining on to $\tilde{D}$, $\tilde{H}$ and $\tilde{I}$: $\nu = \begin{cases} 111240 \\ 111060 \end{cases} - R/(n-0.65)^2$; $n = 3,4,\ldots,15$ [c]												(1189)	Converging to $^2\Pi_{\frac{1}{2}g}$ and $^2\Pi_{\frac{3}{2}g}$ of CO_2^+

CO_2:

[a] Each series is accompanied by a vibrational series separated from the main series by 1274 cm^{-1} which corresponds to $\Delta G_{\frac{1}{2}}$ in the $^2\Sigma_u^+$ state of CO_2^+.

[b] Each member consists of a long progression in ν_1 with spacings similar to those in $^2\Pi_u$ of CO_2.

[c] In addition a vibrational series, 1410–1260 cm^{-1} to shorter wavelengths, has been observed corresponding to the first ΔG in the ground state of CO_2^+.

TABLE 64 (*continued*)

State	Point Group	T_0	Vibrational Frequencies ν_1 ν_2 ν_3	Rotational Constants A_0 B_0 C_0 $r_0(XY)$ $r_0(YZ)$ α	Electron Configuration	Observed Transitions	References	Remarks
CO_2 (*continued*)								
I	$D_{\infty h}$	100040				$I \leftarrow \tilde{X}$ 991 Å	(1189)	
$\tilde{H}$	$D_{\infty h}$	{100650 100570				$\tilde{H} \leftarrow \tilde{X}$ 994 Å	(1189)	
$\tilde{G}$		99331				$\tilde{G} \leftarrow \tilde{X}$ 1007 Å	(1189)	
$\tilde{F}$	$(D_{\infty h})$	96600	1320			$\tilde{F} \leftarrow \tilde{X}$ 1035–969 Å	(1058)(1189)	
$\tilde{E}$	$(D_{\infty h})$	{92360 91830	{1240 1172			$\tilde{E} \leftarrow \tilde{X}$ 1070–1010 Å	(1058)(1189)	A weak and a strong progression
$\tilde{D}$	$D_{\infty h}$	{89111 88535	{1567 1458			$\tilde{D} \leftarrow \tilde{X}$ {1120–1122 Å	(1189)	Very strong, violet shaded bands
$\tilde{C}$	$D_{\infty h}$	{85840 85100	{1165 1270			$\tilde{C} \leftarrow \tilde{X}$ 1170–1130Å	(1058)(1189)	A weak and a strong progression
$\tilde{B}\begin{Bmatrix}{}^1B_1(\Sigma_g^-)\\ {}^1A_1(\Delta_g)\end{Bmatrix}$	(C_{2v})	{73100 72480	(1225)		$\begin{cases}\ldots b_1 a_1^2 a_2^2 b_2^2 a_1\\ \ldots b_1^2 a_1 a_2^2 b_2^2 a_1\end{cases}$	$\tilde{B} \leftarrow \tilde{X}$ 1390–1220 Å	(1021)(604)	Distinct red shaded bands, possibly two systems
$\tilde{A}^1B_2(\Delta_u)$	C_{2v}	46000		5.3 $\bar{B}=0.426$ 1.246 $122° \pm 2°$	$\ldots 1\pi_u^4 a_2^2 b_2 a_1$	$\tilde{A} \leftrightarrow \tilde{X}$ [d]	(1021)(604)(283)	In absorption weak diffuse bands[e]
$\tilde{X}\,{}^1\Sigma_g^+$	$D_{\infty h}$	0	1388.17[f,g] 667.40[f] 2349.16[f]	— 0.39021[h] — 1.1621 180°	$\ldots 4\sigma_g^2 3\sigma_u^2 1\pi_u^4 1\pi_g^4$	Raman and infrared sp.	(1156)(1085)(995)(245)	

CO_2: [d] In absorption 1750–1400 Å, in emission 3800–3100 Å. [e] Overlapped by continuum; in emission carbon monoxide flame bands; see (283).
[f] For the anharmonic constants x_{ik} see (246). [g] Shifted by Fermi resonance with $2\nu_2^0$ which is at 1285.40 cm^{-1}.
[h] $\alpha_1 = 0.00121$, $\alpha_2 = -0.00072$, $\alpha_3 = 0.00309$; $D = 13.5 \times 10^{-8}$.

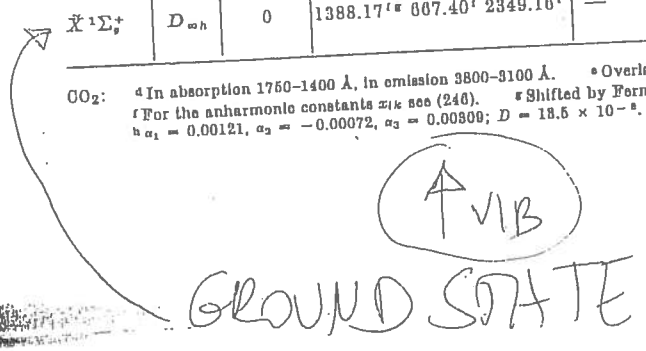

TABLE 64 (*continued*)

$D_0(O_2) \approx D_0(H_2O) = 5.$
(av) 5.1152 eV

State	T_e	ω_e	$\omega_e x_e$	B_e	α_e	D_e (10^{-2}cm^{-1})	r_e (Å)	Observed Transitions: Design.	Observed Transitions: ν_{00}	References
$^1H_2$		$\mu = 0.50391261$		$D_0^0 = 4.4781_3$ eV[a]			I.P. $= 15.4258_9$ eV[b]			NOV 1976 A
		WAVELENGTH TABLES of the H_2 spectrum from 2800 to 29000 Å with assignments of many of the lines (109). The TABLES OF ENERGY LEVELS (24) are also very useful as long as it is realized that the absolute values of the energy levels ($n \geq 2$) relative to the ground state need correction. Graphs and tables of POTENTIAL ENERGY CURVES for all known states of H_2, H_2^+, and H_2^- (107).								
	See v p. 241	Fragments of three other triplet systems.[c]								
u $^3\Pi_u$ 6pπ [123488.$_0$]		Only v=0 observed.		[29.3]		[2.3]	[1.06$_9$]	u→a, δ bands	26232.3[f]	(1)(24)
t[d] $^3\Sigma_u^+$ 5fδ (121292)		(2661.4)	(121.9)	e				t→a,	(25342)	(4)
q[d]($^3\Sigma_g^+$)5dδ (121295)		[2172.6]		e				q→c,	(25325)[f]	(3)
n $^3\Pi_u$ 5pπ 120952.$_9$		2321.4	62.8$_6$	29.9$_5$	1.24[g]	[2.3]	1.057	n→a, γ bands	24847.3[f]	(1)(24)
m[h] $^3\Sigma_u^+$ 4fσ (119317)		[2457.1]		e				m→a,	23295.1[i]	(4)
s $^3\Delta_g$ 4dδ 118875.$_2$		2291.7[j]	62.4$_4$[j]	k				s→c,	22949.3[l]	(1)(18)(24)
r $^3\Pi_g$ 4dπ 118613.$_7$		2280.3[m]	57.9$_6$[m]	k				r→c,	22683.2[m]	(1)(18)(24)
p $^3\Sigma_g^+$ 4dσ 118509.$_8$		2303.1	76.9$_0$	e				p−k,[n]		(154)
								p→c,	22586.0[f]	(1)(18)(24)
v ($^3\Pi_g$)[o] (118330)		(2340)	(57)	([29.1])			([1.07$_2$])	v→c,	(22430)	(3)
k $^3\Pi_u$ 4pπ 118366.$_2$[p]		2344.37	67.2$_9$[q]	30.07$_4$	1.46$_2$[r]	[1.8$_5$]	1.054$_7$	k→a, β bands	22271.0[f]	(1)(15a)(24)
f $^3\Sigma_u^+$ 4pσ (116705)		[2143.6][s]		[27.0][s]			[1.11]	f→a,	20526.0[s]	(1)(24)
o[t] $^3\Sigma_u^+$ (114234)		2399.1	91.0	[35]			[0.98]	o→a,	(18160)	(4)
ι[u] $^3\Pi_u$ 113825		2596.8	106.0	[36]			[0.96]	ι→a,	17846[f]	(4)

State	T_e	ω_e	$\omega_e x_e$	B_e	α_e	D_e (10^{-2} cm^{-1})	r_e (Å)	Observed Transitions: Design.	Observed Transitions: ν_{00}	References
$^1H_2$ (continued)										
B $^1\Sigma_u^+$ 2pσ	91700.0[a]	1358.09	20.888[b]	20.015_4[c]	1.1845[d]	1.625[e]	1.2928_2	$B^f \leftrightarrow X$,[gh] Lyman b.	R 90203.3_5	(25)(77)(129)
X $^1\Sigma_g^+$ $1s\sigma^2$	0	4401.21_3	121.33_6[i]	60.853_0[k]	3.062_2[j]	4.71[l]	0.74144	Quadrupole[m] and field-induced sp..[n]		(15)(48) (26)(56)(74)
		4164 ancient temp i°K gas/liquid						Raman sp.[o]		(23)(56)
		4401.21 − 2(121.33) = 4158.55						Rotational[p] and nuclear rf magn. reson.		(17a)(21) (17)(19)

$^1H_2$: [a] See [n] p. 249.

[b] $+ 0.7196(v+\frac{1}{2})^3 - 0.0598(v+\frac{1}{2})^4 + 0.00216(v+\frac{1}{2})^5$, $Y_{00} = 8.7$; from a least squares fit (129) to the first eight levels as given by (25). (77) gives slightly different constants based on the first five levels only. (73) and (37) have observed levels up to v=35 and 37, resp., very close to the dissociation limit at 118377.$_6$ cm^{-1} (95). The dissociation energy of the B $^1\Sigma_u^+$ state is 28174.2 cm^{-1}.

[c] RKR potential functions (31)(44)(72)(89); see also (126). Precise ab initio potential function (incl. diagonal corrections) and predicted vibrational levels (67)(152).

[d] $+ 0.1214(v+\frac{1}{2})^2 - 0.0117(v+\frac{1}{2})^3 + 0.0004_6(v+\frac{1}{2})^4$, from a least squares fit (129) to the first eight levels. (77) gives slightly different constants based on the first five levels only. For $v \geq 8$ there are strong rotational perturbations caused by interaction with C $^1\Pi_u$. Only after deperturbation can meaningful B_v values for these levels be obtained [see (129)]. For a theoretical discussion of the intensities in the perturbed region see (131).

[e] $- 2.16_5 \times 10^{-3}(v+\frac{1}{2}) + 2.28_9 \times 10^{-4}(v+\frac{1}{2})^2 - 1.18_5 \times 10^{-5}(v+\frac{1}{2})^3$. For individual B_v and D_v values see (25)(37)(129).

[f] Lifetime τ(v=3...7) = 0.8 ns (66); τ(v=8...11) = 1.0 ns (111).

[g] Franck-Condon factors from RKR potentials (51)(89); from ab initio potential functions (64)(90)(91), including theoretical oscillator strengths; see also (167). J dependence of Franck-Condon factors and transition probabilities (87) (88)(102). Experimental Franck-Condon factors and oscillator strengths (57)(65)(69)(83)(130)(142)(157); $\Sigma f_{v'0}$ = 0.29. Variation of transition moment with r (69)(83)(157) and, ab initio, (64)(88). Selective enhancements of v=3 and 10 of B $^1\Sigma_u^+$ in an Ar-H_2 mixture, first observed by Lyman,

State	T_e	ω_e	$\omega_e x_e$	B_e	α_e	D_e ($10^- cm^{-1}$)	r_e (Å)	Observed Transitions: Design.	Observed Transitions: ν_{00}	References
$^{16}O_2$		$\mu = 7.9974575_1$		$D_0^0 = 5.115_6$ eV[a]		I.P.($1\pi_g$) = 12.071 eV[b] ($1\pi_u$) = 16.092 eV[c] ($3\sigma_g$) = 18.159 eV[c] ($2\sigma_u$) = 24.549 eV[c] ($2\sigma_g$) = 39.6 eV[d] ($1s_O$) = 543.1 eV[d]				MAR 1977 A
A detailed review of the entire spectrum of molecular oxygen has been published by (141).										
Potential energy diagrams (63)(128)(141)(190); predicted electronic states and potential functions (167)(176)(182).										
Z ($^3\Pi_u$)		Several Rydberg states converging to the oxygen K limits at 543.1($^4\Sigma^-$) and 544.2($^2\Sigma^-$) eV, in X-ray absorption and electron energy loss spectra. Strong X-ray absorption peak (excitation $1s_O \rightarrow 1\pi_g$).						Z ← X,	532 eV[e]	(133)(166)(175)
Absorption cross sections and cross sections for the production of atomic fluorescence by photodissociation in the region 175 - 850 Å (570000 - 115000 cm^{-1}) (156)(158)(161)(164). Earlier results in (18)(23)(58).										
		Rydberg states with the outer electrons in $3s\sigma$, $3p\sigma$, $3d\sigma$ orbitals and the O_2^+ core in the highest $...1\pi_u^3\,1\pi_g^2\,^2\Pi_u$ state have been tentatively identified in the electroionization spectrum of O_2 at 20.73, 21.75, 22.28 eV, respectively.								(160)
		Codling and Madden's Rydberg series converging to c $^4\Sigma_u^-(v=0)$ of O_2^+ : $\nu = 198125 - \begin{cases} R/(n-0.16)^2 & n = 3\,(Y\ state),4...11.^{fg} \\ R/(n-0.95)^2 & n = 3\,(W\ state),4....8.^{fgh} \end{cases}$ Similar series with v'=1.								(65)*
Y ^{f} (184440)		[1510]		g				Y ← X,	184410	(65)*
W ($^3\Sigma_u^-$)^f (168290)		[1510]		g				W ← X,	168260	(65)*
		Yoshino and Tanaka's weak Rydberg series converging to B $^2\Sigma_g^-(v=0)$ of O_2^+ : $\nu = 163700 - R/(n-0.54)^2$ $n = 6\,(V\ state),7...12.^f$ Similar series with v'=1,2,3.								(98)
V ^{f} (160270)		(1100)						V ← X,	160031	(98)
		Tanaka and Takamine's strong Rydberg s. of R shaded dif. b. converging to B $^2\Sigma_g^-(v=0)$ of O_2^+ : $\nu = 163702 - R/(n-0.70)^2$ $n = 3\,(U\ state),4...23.^{fi}$ Similar series with v'=1,2,3.								(9)(86)*(98)*

State	T_e	ω_e	$\omega_e x_e$	B_e	α_e	D_e	r_e	Observed Transitions	References

State	T_e	ω_e	$\omega_e x_e$	B_e	α_e	D_e (10^{-6} cm^{-1})	r_e (Å)	Observed Transitions: Design.	Observed Transitions: ν_{00}	References
$^{16}O_2$ (continued)										
b $^1\Sigma_g^+$	13195.1	1432.77[a]	z 14.00[a]	1.40037[a]	0.01820[a]	5.351[b]	1.22688	b→a,[c]	5238.5	(40)
								b↔X,[de] R	13120.91[f] z	(12)*
								Atmospheric oxygen b.		
a $^1\Delta_g$	7918.1	[1483.5$_0$]	z (12.$_9$)	1.4264	0.0171	[4.86]	1.2156$_3$	a^g↔X,[he] R	7882.39 z	(10)*
								IR atmosph. oxygen b.		
X $^3\Sigma_g^-$	0	1580.19$_3$	z 11.98$_1$[i]	[1.4376766][j] B_e = 1.44563	0.0159$_3$[kℓ]	[4.839][jℓ]	1.20752	Rot.-vibr. sp. (collision induced)		(12a)(75a) (142)
								Rotation sp.[mn]		(94)(105)
								Spin reorientation (fine structure) sp.[mo]		(20)(41)(76) (120)(159)
								Raman sp.[p]		(38)* (124)* (162)(183)*
								EPR sp.		(25)(138)(154)

O_2:

[a] These constants have been re-evaluated [(148), see also (168)] from the measurements of the b−X system (12) using improved lower state constants; $\gamma_e = -0.000004_2$. RKR potential curve (148). Constants for $^{16}O^{18}O$, $^{16}O^{17}O$ in (12).

[b] $+ 0.0318(v+\frac{1}{2}) + 0.0012(v+\frac{1}{2})^2$. The D_v values have been calculated (148) using vibrational wavefunctions computed from the experimental potential curve; see (147).

[c] Q branch of the 0-0 band observed in a discharge through O_2 and He. Absolute transition probability $\sim 2.5 \times 10^{-3}$ s^{-1}.

[d] In absorption observed in the solar spectrum; in the laboratory with more than 1 m path. In emission in the aurora and nightglow (14) as well as in various discharges (11) (15)(39)(40). Band intensities [in cm^{-1}km^{-1}atm^{-1}(STP)] for the 0-0, 1-0, 2-0 bands are 532, 40.8, 1.52, respectively (102); slightly smaller values in (137). The transition probability for the 0-0 band is 0.075 s^{-1} [average of values given by (102) and (137)]. (49) gives the band oscillator strengths $f_{00} = 2.5 \times 10^{-10}$, $f_{10} \approx 0.2 \times 10^{-10}$. RKR Franck-Condon factors (141)(190); rotational intensity distribution and pressure broadening (100)(102)(137).

[e] Pressure induced spectra a←X, b←X as well as simultaneous transitions in two colliding molecules have been studied by many investigators. See recent papers by (116)(142) which refer to earlier work.

[f] (148) give $\nu_{00} = 13122.235$ cm^{-1}, differing by $+\frac{2}{3}\lambda$ (spin-spin interaction in X $^3\Sigma_g^-$) from the zero line of (12).

State	T_e	ω_e	$\omega_e x_e$	B_e	α_e	D_e (10^{-} cm^{-1})	r_e (Å)	Observed Transitions: Design.	Observed Transitions: ν_{00}	References
$^{14}N_2$		μ = 7.00153720		D_0^0 = 9.759$_4$ eV[a]						FEB 1977 A

I.P.($3\sigma_g$) = 15.5808 eV[b]
($1\pi_u$) = 16.6986 eV[bc]
($2\sigma_u$) = 18.7507 eV[b]
($2\sigma_g$) = 37.9 eV[d]
($1s_N$) = 409.9$_8$ eV[e]

For a very detailed and critical review of the spectrum of molecular nitrogen and its ions see the recent publication by Lofthus and Krupenie (196). Atlas of the VUV absorption spectrum 1060 - 1520 Å and table of absorption lines (87). Tables of band head wavelengths (39)(48)(196). Photoionization and absorption cross sections (45)(57)(147). Potential functions (60)(68)(182)(196).

$x''(^1\Sigma_u^+)$	Several Rydberg series (excitation of $1s_N$) with limit (K edge) at 409.5 eV.			
$x'(^1\Pi_u)$	X-ray absorption ($3s\sigma \leftarrow 1s_N$).			
	X-ray absorption and emission ($1\pi_g \leftrightarrow 1s_N$), broad peak.[f]	$x'' \leftarrow X$,	405.5$_9$ eV	(114)(166) (173)(174)
		$x' \leftrightarrow X$,	400.8$_4$ eV	
	Photoionization and dissociative photoionization processes corresponding to various excited states of N_2^+.[g]			(177)(194)
$v\ ^1\Pi_g$	From high-energy electron impact spectroscopy.	$v \leftarrow X$,	253000	(180)
u_5 (183640)	Fragments of other progressions and unassigned bands, 198000 - 207000 cm^{-1}.			
u_4 (178565)	(2100) (15) (2070) (15) First two members of Codling's Rydberg series.[h]	$u_5 \leftarrow X$,	(183510)	(76)(163)
		$u_4 \leftarrow X$,	(178420)	
$\ldots 2\sigma_u\, 1\pi_u^4\, 3\sigma_g^2 \{ns\sigma / nd\sigma\}$	Hopfield's Rydberg series converging to B $^2\Sigma_u^+(v=0)$ of N_2^+; $\nu = 151233 - \{R/(m+0.141-0.199/m)^2$, m = 3...11 (apparent emission series)[i]; $R/(m-0.070-0.041/m)^2$, m = 3...20 (absorption series)[jkl]			(1)(4)* (37)*
$\ldots 2\sigma_u^2\, 1\pi_u^3\, 3\sigma_g^2\, ns\sigma$	Worley's ("third") Rydberg series joining on to o_3, o_4, o_5 and converging to A $^2\Pi_{u\frac{1}{2}}(v=0)$ of N_2^+; $\nu = 134721 - R/(n-1.06)^2$, n = 3...16.[mnop]			(8)(37)* (190)*
$\ldots 2\sigma_u^2\, 1\pi_u^3\, 3\sigma_g^2\, ns\sigma$ [q]	Ogawa and Tanaka's Rydberg series joining on to o_4, o_5 and converging to A $^2\Pi_{u\frac{1}{2}}(v=0)$ of N_2^+; $\nu = 134644 - R/n^{*2}$, n* = 2.84, 3.85, 4.86, ..., 14.91.[mnop]			(37)* (190)*
	Several dissociation continua in the region 100000 - 160000 cm^{-1}.			(105)(156)
	Several unidentified bands in the region 126100 - 131550 cm^{-1}.			(51)

State	T_e	ω_e	$\omega_e x_e$	B_e	α_e	D_e	r_e	Observed Transitions	References

State	T_e	ω_e	$\omega_e x_e$	B_e	α_e	D_e (10^{-6} cm^{-1})	r_e (Å)	Observed Transitions: Design.	Observed Transitions: ν_{00}	References
$^{14}N_2$ (continued)										
B' $^3\Sigma_u^-$	66272.4_7	1516.88	z 12.18_1[a]	1.473_3[b]	0.0166_6[c]	(5.56)	1.278_4	B'→B, R "Y" bands,[d]	6545.5 (z)	(32)(36) (182)
W $^3\Delta_u$	59808	$1501._4$	(z) 11.6					B'↔X,[e] R	65852.35 z	(30)* (35) (66)* (149) (155)
								Ogawa-Tanaka-Wilkinson b.		
								W↔B, R,V	73	(102)(124) (131)(157)
								Wu-Benesch b.		
B $^3\Pi_g$	59619.3_5[g]	1733.39	z 14.122[h]	1.6374_5[i]	0.0179_1[j]	[5.9]	1.2126_0	W←X,[f] R	59380	(123)* (155)
								Saum-Benesch b.		
								B^k↔A,[l] V	9552.0_3 z	(29)(196)
								lst pos. gr.		
A $^3\Sigma_u^+$	50203.6_3	1460.64	z 13.87_2[n]	1.4546[o]	0.0180[p]	$[6.1_5]$	1.2866	B←X,[m] R	59306.81 z	(40)
								Wilkinson b.		
X $^1\Sigma_g^+$	0	2358.57	z 14.324[r]	1.99824_1[s]	0.017318[s]	[5.76]	1.09768_5	A^q↔X,[m] R	49754.78 z	(29)(70)(85)
								Vegard-Kaplan b.		
								Rot.-vibr.[t] and rot. sp.:		
								- pressure induced		(14)(59)(63) (86)(135) (141)(181)
								- el. field induced		(185)
								Raman spectra[u]		(20)(134) (167)
								Mol. beam magn. reson.[v]		

N_2: [a] $\omega_e y_e = +0.0418_6$, $\omega_e z_e = -0.000732$ (196).
[b] Spin splitting constants (v=5): $\lambda = +0.66$, $\gamma = -0.0030$ (66).
[c] $\gamma_e = +0.000009$ (196).
[d] Also referred to as "infrared afterglow bands".
[e] RKR Franck-Condon factors (75)(196). Rotational intensity distribution (120).
[f] Franck-Condon factors (123).
[g] $A_e = 42.24$ (133).

N_2 (continued):
[h] $\omega_e y_e = -0.0569$, $\omega_e z_e = +0.00361$ (196); slightly different
[s] From B_v and B_v of (167) and

State	T_e	ω_e	$\omega_e x_e$	B_e	α_e	D_e (10^{-4} cm^{-1})	r_e (Å)	Observed Transitions: Design.	Observed Transitions: ν_{00}	References
$^1H^{81}Br$		μ = 0.99542702		D_0^0 = 3.758 eV[a]		I.P. = 11.67 eV[b]				DEC 1976 A
		Numerous absorption bands above 114000 cm^{-1}, tentatively assigned to higher members of two Rydberg series starting with L and M and converging to A $^2\Sigma^+$ of HBr^+; I.P.[$A^2\Sigma^+$,v=0] = 123373 cm^{-1} (15.296$_4$ eV).								(43)
M ($^1\Sigma^+$) (109473)		[1308]		v=0...4 observed. Assigned as $4p\sigma\,4p\pi^4\,6s\sigma$.[c]				M← X,	108814	(43)*
L ($^1\Sigma^+$,$^1\Pi$) (104201)		[1262]		v=0...3 observed. Assigned as $4p\sigma\,4p\pi^4\,5p\sigma$ and/or $5p\pi$.[c]				L← X,	103519	(43)*
		Further absorption bands of doubtful assignment between 75200 and 83600 cm^{-1}.								(13)(15)
K[d] 1 (83902)		(2518)[e]		[8.195]		[22.0]	[1.437$_5$]	K← X,	R 83847.9[f] z	(15)
J[d] 1 (81243)		(2502)[e]		[8.02$_7$][g]		[3.6$_1$]	[1.453]	J← X,	R 81180.7[h] z	(13)*
I[d] 1 (80436)		(2525)[e]		[8.16$_9$][i]		[10.$_4$]	[1.440]	I← X,	R 80385.6[j] z	(13)*
g ($^3\Sigma^-$)0$^+$ t [79253.2]				[7.6$_3$][k]		[-17]	[1.49]	g← X,	R 77940.$_0$ z	(13)* (36)*
F $^1\Delta$ t [78322.3]				[8.20]			[1.43$_7$]	F← X,	R 77009.1 z	(36)*
f_1 $^3\Delta_1$ t (76814)		[2299.7]	z	8.02$_7$	0.21$_3$		1.453	f_1← X,	R 76650.9 z	(13)(36)*
D $^1\Pi$ u (76310)		[2405.5]	z	8.12$_5$	0.21		1.444	D← X,	R 76199.4 z	(13)* (36)*
d_0 $^3\Pi_0$ u (76193)		[2418.5]	z	[7.624][l]	(0.32)		[1.490$_4$]	d_0← X,	R 76088.8 z	(13)(36)*
E ($^1\Sigma^+$)0$^+$ t [76691]				[7.34][m]			[1.51$_9$]	E← X,	R 75378	(36)
V $^1\Sigma^+$ n (75800)		(790)		Bands in emission above 46500 cm^{-1}, in absorption above 75700. Incomplete analysis.				V↔ X,[o]	R (74900)	(14)(36)*
f_2 $^3\Delta_2$ t [75533.8]				[8.67$_5$][p]		[16.$_5$][p]	[1.397]	f_2← X,	R 74220.6 z	(13)(36)*
f_3 $^3\Delta_3$ t [75403.1]		Weak transition.		[7.41]		[-7.6]	[1.51$_2$]	f_3← X,	R 74089.9 z	(36)*
e $^3\Sigma^+$ t [75053]		Very diffuse, unresolved band.						e← X,	R 73740	(36)
d_1 $^3\Pi_1$ u [74855]		Diffuse band, rotational structure unresolved.						d_1← X,	R 73542	(13)(36)
d_2 $^3\Pi_2$ u [74753]		Diffuse band, rotational structure unresolved.						d_2← X,	R 73440	(13)(36)

State	T_e	ω_e	$\omega_e x_e$	B_e	α_e	D_e (10^{-4} cm^{-1})	r_e (Å)	Observed Transitions: Design.	Observed Transitions: ν_{00}	References
$^1H^{81}Br$ (continued)										
C $^1\Pi$	ν 70578	2552 Z	52	7.89	0.30		1.46_5	C← X,[q] R	70527.6 Z	(13)(32)*
b_0 $^3\Pi_0$	0^+ ν (68998)	[2452]		$[7.99_6]$[r]			[1.455]	b_0← X, R	68911.2 Z	(13)(32)*
	0^- ν (68991)							R	68904[s] H	
b_1 $^3\Pi_1$	ν (67180)	[2444.2] Z		8.14_8[r]	0.29_2		1.442	b_1← X, R	67088.4 Z	(13)* (32)*
b_2 $^3\Pi_2$	ν [67663.0]			$[7.80_5]$[r]			[1.473]	b_2← X, R	66349.8 Z	(13)(32)*

[1]HBr: [a]From $D_0^0(H_2)$, $D_0^0(Br_2)$, and ΔH_{f0}(HBr; from gaseous H_2, Br_2).
[b]Average value from photoionization (10) and photoelectron spectra (23)(29); refers to X $^2\Pi_{3/2}$ of the ion. A more recent paper (39) gives 11.64_5 eV.
[c]Strongly broadened by preionization; estimated lifetime against preionization 9.5×10^{-15} s (46).
[d]I, J, K correspond to absorption bands with clear analogues in DBr.
[e]From the observed HBr-DBr isotope shift assuming that the observed bands are 0-0 bands.
[f]Band [37] of (15).
[g]Λ-type doubling, $\Delta\nu_{ef} = + 0.14_2 \times J(J+1) - \ldots$; B and D represent average values.
[h]Band [28] of (13). Sharp P, Q, R branches; the Q levels appear to be predissociated for $J \geq 14$.
[i]From R, P branches. $\Delta\nu_{ef} = - 0.041 \times J(J+1)$.
[j]Band [26] of (13).
[k]Perturbed at high J.
[l]Slightly diffuse lines.
[m]Perturbed.
[n]Derived from $H^+ + Br^-$; configuration $\ldots\sigma\pi^4\sigma^*$.
[o]Heavily perturbed extensive band system. Absorption lines above 75923 cm^{-1} are diffuse. B' varies irregularly between 3.4 and 4.5 cm^{-1}.
[p]Average values for the two Λ-type doubling components.
[q]Very strong absorption, lines are diffuse.
[r]Diffuse rotational structure.
[s]Diffuse Q head.
[t]Configuration $\ldots\sigma^2\pi^3 5p\pi$.
[u]Configuration $\ldots\sigma^2\pi^3 5p\sigma$.
[v]Configuration $\ldots\sigma^2\pi^3 5s\sigma$.

State	T_e	ω_e	$\omega_e x_e$	B_e	α_e	D_e (10^{-4} cm^{-1})	r_e (Å)	Observed Transitions: Design.	Observed Transitions: ν_{00}	References
$^1H^{81}Br$ (continued)										
A ($^1\Pi$)	w	Continuous absorption starting at ~35000 with maximum at 56400 cm^{-1}.								
X $^1\Sigma^+$	0	2648.975[x]	z 45.217$_5$[y]	8.46488$_4$[x]	0.23328[z]	3.457$_5$[a']	1.41443$_5$	A ← X		(1)(2)(4)(5)(28)
								Rot.-vibr. sp.[b'c']		(21)
								Rotation spectrum[d'c']		(8)(17)(31)
								Raman sp.[e']		(45)
								Mol. beam el. reson.[f']		(42)

^{1}HBr (continued):

[w] Configuration $\ldots\sigma^2\pi^3\sigma^*$.

[x] These are Y_{10} and Y_{01} values; applying Dunham corrections (21) obtain $\omega_e = 2649.21_5$, $B_e = 8.46506_5$. Additional corrections (adiabatic, non-adiabatic) are discussed by (38). The microwave B_0 value of (17) was included in the evaluation of B_e. See also b'f'.

[y] $\omega_e y_e = -0.0029$.

[z] $+ 0.000873_5(v+\frac{1}{2})^2 - 0.000120(v+\frac{1}{2})^3$.

[a'] $- 0.039_7 \times 10^{-4}(v+\frac{1}{2}) + 0.0038(v+\frac{1}{2})^2$;

[b'] $H_v = 7.63 \times 10^{-9} - 0.55 \times 10^{-9}(v+\frac{1}{2})$.

[b'] In absorption the 1-0, 2-0, 3-0, 3-1, 4-0, 5-0, 6-0 bands have been studied (6)(7)(12)(21)(41); in emission 1-0, 2-1, 3-2, 4-3 (11)(20). The constants in the table are from (21), those of (20)(41) are very similar and of comparable accuracy. See also (47). Absolute intensities have been measured (16)(18)(30)(33) and the dipole moment function has been calculated; (40) give for $H^{79}Br$ [D,Å]: $\mu_{e\ell}(r) = +0.788 + 0.315(r-r_e) + 0.575(r-r_e)^2$; see also (24)(34)(37).

[c'] For observations and measurements of pressure-induced bands and pure rotation lines ($\Delta J=2$) see (22)(27). The pressure broadening of the lines has been studied by (16)(25).

[d'] Absolute intensities have been measured by (19).

[e'] Raman cross sections in gaseous HBr.

[f'] The following constants (as well as corresponding values for $H^{79}Br$) are given in (42):

- $\mu_{e\ell}(v=0,J=1) = 0.8265$ D [in a later paper (44) derive 0.8282 D from Stark effect of rotation spectrum];
- quadrupole and other hyperfine coupling constants;
- $g_J = 0.3712$.

These constants supersede earlier values of (9)(17)(26)(31)(35).

State	T_e	ω_e	$\omega_e x_e$	B_e	α_e	D_e (10^{-4} cm^{-1})	r_e (Å)	Observed Transitions: Design.	Observed Transitions: ν_{00}	References
$^2H^{81}Br$		μ = 1.96518641	D_0^0 = 3.804 eV[a]	I.P. = 11.67$_3$ eV[b]						DEC 1976 A
		Numerous absorption bands above 114000 cm^{-1}; see ^{1}HBr.								(13)
M ($^1\Sigma^+$)	(109374)	[1000] v=0...5 observed. } See ^{1}HBr.						M← X,	108937	(13)*
L ($^1\Sigma^+$,$^1\Pi$)	(104141)	[971] v=0...4 observed. }						L← X,	(103690)	(13)*
		Further absorption bands of doubtful assignment between 72000 and 83800 cm^{-1}.								(6)
K[c] 1	(83908)	(1792)[d]		[4.121]$_4$[e]		[0.80]	[1.442$_8$]	K← X, R	83867.1[f] Z	(6)
J[c] 1	(81248)	(1781)[d]		[4.083][g]		[1.36]	[1.449$_5$]	J← X, R	81202.2[f] Z	(6)*
I[c] 1	(80442)	(1797)[d]		[4.107]		[1.38]	[1.445$_2$]	I← X, R	80403.8[f] Z	(6)
g ($^3\Sigma^-$)0$^+$	(78125)	[1440.$_6$]	Z	[3.79]	(0.40)[h]	[14]	[1.50$_4$]	g← X, R	77908.8 Z	(6)(10)
F $^1\Delta$	[77989.0]			[4.095]			[1.447$_3$]	F← X, R	77052.3 Z	(6)(10)
f_1 $^3\Delta_1$	(76787)	[1657.3]	Z	4.06$_4$	0.07$_6$		1.453	f_1← X, R	76679.2 Z	(6)(10)
D $^1\Pi$	(76280)	[1732.6]	Z	4.128[i]	0.076		1.441$_5$	D← X, R	76209.1 Z	(6)(10)*
d_0 $^3\Pi_0$	[77027.4]			[3.99$_3$][j]			[1.466]	d_0← X, R	76090.7 Z	(10)*
E ($^1\Sigma^+$)0$^+$	(75682)	[1365]	Z	[3.953]	(0.78)[h]		[1.472$_9$]	E← X, R	75428.1 Z	(6)(10)
V $^1\Sigma^+$		Extensive absorption system above 75700 cm^{-1}, incompletely analysed because of strong perturbations. B_v values range from 1.68 to 2.12.						V← X, R		(10)
f_2 $^3\Delta_2$	(74370)	[1660.3]	Z	4.29$_4$	0.097	[2.4]	1.413	f_2← X, R	74263.1 Z	(6)(10)*
f_3 $^3\Delta_3$	[75088.6]	Weak transition.		[3.83]		[-2.1]	[1.49$_7$]	f_3← X, R	74151.9 Z	(10)*
e $^3\Sigma^+$	[74677]	Very diffuse, unresolved band.						e← X,	73740	(10)
d_1 $^3\Pi_1$	[74499]	Diffuse band, rotational structure unresolved.						d_1← X, R	73562	(6)(10)
d_2 $^3\Pi_2$	[74391.5]			[3.906][k]		[0.36]	[1.482]	d_2← X, R	73454.8 Z	(6)(10)*
C $^1\Pi$	70563	1811.2	Z 25.5	4.02[l]	0.10$_5$		1.46$_1$	C← X, R	(70501) H[Q]	(6)(8)*

State	T_e	ω_e	$\omega_e x_e$	B_e	α_e	D_e (10^{-4} cm^{-1})	r_e (Å)	Observed Transitions: Design.	Observed Transitions: ν_{00}	References
$^2H^{81}Br$ (continued)										
b_0 $^3\Pi_0$ 0^+	[69837.1]			$[4.08_2]^m$			[1.450]	$b_0 \leftarrow X$,	R 68900.4 Z R (68895)	(6)* (8)*
$^3\Pi_0$ 0^-	[69832]	Unresolved Q branch, assignment uncertain.								
b_1 $^3\Pi_1$	67113.$_9$	1814	Z 27	4.10^n	0.09		1.44_6	$b_1 \leftarrow X$,	R 67077.5 Z	(6)(8)
b_2 $^3\Pi_2$	[67290.7]			$[4.01_8]^m$			[1.461]	$b_2 \leftarrow X$,	R 66354.0 Z	(6)(8)
A ($^1\Pi$)		Continuous absorption beginning at ~39000 cm^{-1}.						A ← X,		(1)
X $^1\Sigma^+$	0	1884.75	Z 22.71$_8$ ^{o}	$[4.245596]^p$	0.083$_8$	$[0.8832]^p$	1.4145	Rot.-vibr. sp.^{q}		(2)(5)
		637.33 = 1884.75 - 2(23.71)						Rotation spectrum^r		(3)(4)(9)(12)

^{2}HBr: ^{a}From D_0^0(^{1}HBr).
^{b}From the photoelectron sp. (11) of the isotopic mixture.
^{c}See ^{d} of ^{1}HBr.
^{d}See ^{e} of ^{1}HBr.
$^e\Omega$-type doubling, $\Delta\nu_{ef} \approx + 0.0371\,J(J+1)$.
^{f}Bands {35}, {27}, {26} of (6).
$^g\Omega$-type doubling, $\Delta\nu_{ef} = + 0.0314\,J(J+1)$.
^{h}v=0 and 1 only; v=1 is perturbed.
^{i}From P, R branches. $B_0(Q) = 4.109$.
^{j}From P, R branches. $B_0(Q) = 3.92_6$.
^{k}Branches are slightly diffuse.
$^\ell$Diffuse rotational structure; v=0...4.
^{m}Slightly diffuse lines.
^{n}v=2, 3 diffuse. Slightly diffuse lines for v=0, 1.
$^o\omega_e y_e = - 0.010_6$.
^{p}Microwave value (9)(12).
^{q}1-0, 2-0, 3-0 bands in absorption (2), Δv=1 sequence in emission (5).
$^r\mu_{e\ell}$(v=0) = 0.8233 D from Stark effect of 1-0 line (12).
Quadrupole and other hyperfine coupling const. (7)(9)(12).

(1) See ref. (1) of ^{1}HBr.
(2) Keller, Nielsen, JCP 22, 294 (1954).
(3) Palik, JCP 23, 217 (1955).
(4) Cowan, Gordy, PR 111, 209 (1958)
(5) See ref. (11) of ^{1}HBr.
(6) See ref. (15) of ^{1}HBr.
(7) See ref. (26) of ^{1}HBr.
(8) See ref. (32) of ^{1}HBr.
(9) De Lucia, Helminger, Gordy, PR A 3, 1849 (1971).
(10) See ref. (36) of ^{1}HBr.
(11) See ref. (39) of ^{1}HBr.
(12) See ref. (44) of ^{1}HBr.
(13) See ref. (43) of ^{1}HBr.

TABLE 16.3
van der Waals constants for various substances.

Species	$a/\text{dm}^6\cdot\text{bar}\cdot\text{mol}^{-2}$	$a/\text{dm}^6\cdot\text{atm}\cdot\text{mol}^{-2}$	$b/\text{dm}^3\cdot\text{mol}^{-1}$
Helium	0.034598	0.034145	0.023733
Neon	0.21666	0.21382	0.017383
Argon	1.3483	1.3307	0.031830
Krypton	2.2836	2.2537	0.038650
Hydrogen	0.24646	0.24324	0.026665
Nitrogen	1.3661	1.3483	0.038577
Oxygen	1.3820	1.3639	0.031860
Carbon monoxide	1.4734	1.4541	0.039523
Carbon dioxide	3.6551	3.6073	0.042816
Ammonia	4.3044	4.2481	0.037847
Methane	2.3026	2.2725	0.043067
Ethane	5.5818	5.5088	0.065144
Ethene	4.6112	4.5509	0.058199
Propane	9.3919	9.2691	0.090494
Butane	13.888	13.706	0.11641
2-Methyl propane	13.328	13.153	0.11645
Pentane	19.124	18.874	0.14510
Benzene	18.876	18.629	0.11974

$a = 2.3026\ \text{dm}^6\cdot\text{bar}\cdot\text{mol}^{-2}$ and $b = 0.043067\ \text{dm}^3\cdot\text{mol}^{-1}$ for methane. If we divide Equation 16.5 by $\overline{V} - b$ and solve for P, we obtain

$$\begin{aligned} P &= \frac{RT}{\overline{V} - b} - \frac{a}{\overline{V}^2} \\ &= \frac{(0.083145\ \text{dm}^3\cdot\text{bar}\cdot\text{mol}^{-1}\cdot\text{K}^{-1})(273.15\ \text{K})}{(0.250\ \text{dm}^3\cdot\text{mol}^{-1} - 0.043067\ \text{dm}^3\cdot\text{mol}^{-1})} - \frac{2.3026\ \text{dm}^6\cdot\text{bar}\cdot\text{mol}^{-2}}{(0.250\ \text{dm}^3\cdot\text{mol}^{-1})^2} \\ &= 72.9\ \text{bar} \end{aligned}$$

By comparison, the ideal-gas equation predicts that $P = 90.8$ bar. The prediction of the van der Waals equation is in much better agreement with the experimental value of 78.6 bar than is the ideal-gas equation.

The van der Waals equation qualitatively gives the behavior shown in Figures 16.3 and 16.4. We can rewrite Equation 16.5 in the form

$$Z = \frac{P\overline{V}}{RT} = \frac{\overline{V}}{\overline{V} - b} - \frac{a}{RT\overline{V}} \tag{16.6}$$

TABLE 16.4
The Redlich-Kwong equation parameters for various substances.

Species	$A/\text{dm}^6\cdot\text{bar}\cdot\text{mol}^{-2}\cdot\text{K}^{1/2}$	$A/\text{dm}^6\cdot\text{atm}\cdot\text{mol}^{-2}\cdot\text{K}^{1/2}$	$B/\text{dm}^3\cdot\text{mol}^{-1}$
Helium	0.079905	0.078860	0.016450
Neon	1.4631	1.4439	0.012049
Argon	16.786	16.566	0.022062
Krypton	33.576	33.137	0.026789
Hydrogen	1.4333	1.4145	0.018482
Nitrogen	15.551	15.348	0.026738
Oxygen	17.411	17.183	0.022082
Carbon monoxide	17.208	16.983	0.027394
Carbon dioxide	64.597	63.752	0.029677
Ammonia	87.808	86.660	0.026232
Methane	32.205	31.784	0.029850
Ethane	98.831	97.539	0.045153
Ethene	78.512	77.486	0.040339
Propane	183.02	180.63	0.062723
Butane	290.16	286.37	0.08068
2-Methyl propane	272.73	269.17	0.080715
Pentane	419.97	414.48	0.10057
Benzene	453.32	447.39	0.082996

where A, B, α, and β, are parameters that depend upon the gas. The values of A and B in the Redlich-Kwong equation are listed in Table 16.4 for a variety of substances. The parameter α in the Peng-Robinson equation is a somewhat complicated function of temperature, so we will not tabulate values of α and β. Equations 16.7 and 16.8, like the van der Waals equation (Example 16–2), can be written as cubic equations in $\overline{V}$. For example, the Redlich-Kwong equation becomes (Problem 16–26)

$$\overline{V}^3 - \frac{RT}{P}\overline{V}^2 - \left(B^2 + \frac{BRT}{P} - \frac{A}{T^{1/2}P}\right)\overline{V} - \frac{AB}{T^{1/2}P} = 0 \qquad (16.9)$$

Problem 16–28 has you show that the Peng-Robinson equation of state is also a cubic equation in $\overline{V}$.

EXAMPLE 16–3
Use the Redlich-Kwong equation to calculate the molar volume of ethane at 300 K and 200 atm.

EXPERIMENT 41

Computational Determination of the Molecular Constants of HCl

Objective

Calculation of the molecular constants of HCl using ab initio quantum mechanical methods.

Introduction

Experiment 36 guides you through the acquisition and analysis of the infrared spectrum of gaseous HCl with the goal of obtaining its molecular constants. It is helpful to review here the ultimate objective of that experiment in terms of the five molecular constants sought. These constants are (1) the harmonic frequency, $\tilde{\nu}_e$; (2) the anharmonicity constant, $\tilde{\nu}_e\chi_e$; (3) the rotational constant, B_e; (4) the rotation–vibration coupling constant, α_e; and (5) the centrifugal distortion constant, D.

This experiment has the same objective. However, you will not use a traditional "experimental" approach that relies on getting data from a spectrophotometer; instead you will employ computational methods that are based on quantum chemistry. The term "ab initio" cited in the Objective means "from the beginning," and it may be interpreted that you will obtain these results from an entirely mathematical quantum mechanical calculation. The goal of these approaches is to obtain solutions to the Schrödinger equation by making as few approximations as possible and by avoiding the use of adjustable parameters.

You will use some of the most advanced and reliable techniques currently available in standard computational chemistry applications. The methods to be used do not rely on any expeditious assumptions (or adjustable parameters) to facilitate or even permit the calculations to be made. Moreover, these calculations can be performed on a stand-alone personal computer. Thus, you are the beneficiary of forty years of research in quantum chemistry, immense advancements in computing power, and the successful efforts of computer programmers.

The quality of the results that can be achieved for small molecules (such as diatomics) using advanced quantum chemical calculations permits one to determine molecular constants to within one percent of the experimental quantities. This achievement is particularly significant because one can now calculate the molecular constants and thus predict the rotational–vibrational spectra of unstable or exotic species.

Computational Approach

Before we present the computational details, we will give you the basic outline of the approach to be followed in this experiment. The strategy is to obtain the internuclear potential energy (PE) function of HCl in the vicinity of the potential minimum, for it is the shape of the PE function in this region that determines the five molecular constants mentioned. Figure 1 shows a qualitative example of the PE function of a diatomic molecule and the portion of the curve that we strive to calculate.

In *Step 1*, we will use high-level quantum chemical methods to calculate the electronic energy of HCl at specifically chosen internuclear separations. Then in *Step 2* we will refine these energies using a computational technique called *basis set extrapolation*. In *Step 3* we will fit these refined PE points to a sixth-order

The second line indicates that the Cl atom is attached to atom 1 (H) at a distance r. The third line is blank. The last line, used in concert with the scan keyword, tells the program to start with a value of r = 1.0 Å, perform the calculation indicated in the Route Section, then increment r by 0.1 Å, and repeat the calculation. This process is carried out for a total of eight 0.1-Å steps, thus producing a scan consisting of 9 points along the H–Cl internuclear potential energy surface.

After this calculation, carry out two additional scans using the triple and quadruple zeta basis sets. Simply replace the "d" in the basis set in the Route Section by "t" and then "q". The other parts of the input file remain the same (except for the entries in the Title Sections).

Step 2

Now we will use the results from Step 1 to obtain the CBS-extrapolated energies for *each* of the nine points along the PE curve. Although the results of the scan are summarized in the Gaussian output file, the energies reported there are unfortunately not formatted to sufficient significant figures. Therefore you will have to copy the numerical results from the very end of the file, paste them into a word processor, and arrange them in a single, continuous line with the values separated by commas (don't worry about soft line returns). The results of the double zeta scan, as they appear in the output file, are shown in the Appendix of this experiment. Save this data as an ASCII-delimited text file. Import the file to Excel/SDAS, using the commas to delimit the values from each other so that they occupy separate cells in a row. In a similar fashion, transfer the CCSD(T) data from the triple and quadruple zeta scans to this spreadsheet so that the three energies for a given H–Cl distance are aligned in a column. Enter the numbers 2, 3, and 4 into another column, and use SDAS to obtain the CBS energies for each H–Cl scan point, just as you did in the exercise with helium. This process is less tedious than it might seem because SDAS recalls the user-defined function during a session. You can use the same values—$E_{CBS} = -409$ and $b = c = 1$—for the initial guesses of the parameters in these analyses.

After you complete each CBS extrapolation, copy the CBS energy from the SDAS *Model* sheet and paste it into your working spreadsheet (you must use *Paste Special—Values*). Arrange these CBS values in a column. Enter the respective H–Cl distances (in Å units) in the cells to the left of the CBS energies. Plot your data; if all went well, your graph should resemble the bold portion of the curve in Figure 1.

Step 3

Fit your (*E*,*r*) data to the sixth-order polynomial

$$E(r) = a_0 + a_2(r - r_e)^2 + a_3(r - r_e)^3 + a_4(r - r_e)^4 + a_5(r - r_e)^5 + a_6(r - r_e)^6, \quad (4)$$

which has seven parameters. The reason that we use such an extensive function is that it is able to capture accurately the curvature of the PE function in the vicinity of the minimum and thus yield accurate values of the desired molecular constants. The first parameter, a_0, sets the energy at the minimum of the function, where $r = r_e$. The second-order constant, a_2, accounts for the harmonic (parabolic) character of the PE function, and the remaining constants describe the anharmonic quality of the potential. As we will see in Step 4, the molecular constants can be extracted from these constants.

Fit your CBS scan energies to equation (4). You will probably need initial guess values of the parameters. You can easily estimate a_0 and r_e from the position of

The second line indicates that the Cl atom is attached to atom 1 (H) at a distance r. The third line is blank. The last line, used in concert with the scan keyword, tells the program to start with a value of r = 1.0 Å, perform the calculation indicated in the Route Section, then increment r by 0.1 Å, and repeat the calculation. This process is carried out for a total of eight 0.1-Å steps, thus producing a scan consisting of 9 points along the H–Cl internuclear potential energy surface.

After this calculation, carry out two additional scans using the triple and quadruple zeta basis sets. Simply replace the "d" in the basis set in the Route Section by "t" and then "q". The other parts of the input file remain the same (except for the entries in the Title Sections).

Step 2

Now we will use the results from Step 1 to obtain the CBS-extrapolated energies for *each* of the nine points along the PE curve. Although the results of the scan are summarized in the Gaussian output file, the energies reported there are unfortunately not formatted to sufficient significant figures. Therefore you will have to copy the numerical results from the very end of the file, paste them into a word processor, and arrange them in a single, continuous line with the values separated by commas (don't worry about soft line returns). The results of the double zeta scan, as they appear in the output file, are shown in the Appendix of this experiment. Save this data as an ASCII-delimited text file. Import the file to Excel/SDAS, using the commas to delimit the values from each other so that they occupy separate cells in a row. In a similar fashion, transfer the CCSD(T) data from the triple and quadruple zeta scans to this spreadsheet so that the three energies for a given H–Cl distance are aligned in a column. Enter the numbers 2, 3, and 4 into another column, and use SDAS to obtain the CBS energies for each H–Cl scan point, just as you did in the exercise with helium. This process is less tedious than it might seem because SDAS recalls the user-defined function during a session. You can use the same values—$E_{CBS} = -409$ and $b = c = 1$—for the initial guesses of the parameters in these analyses.

After you complete each CBS extrapolation, copy the CBS energy from the SDAS *Model* sheet and paste it into your working spreadsheet (you must use *Paste Special—Values*). Arrange these CBS values in a column. Enter the respective H–Cl distances (in Å units) in the cells to the left of the CBS energies. Plot your data; if all went well, your graph should resemble the bold portion of the curve in Figure 1.

Step 3

Fit your (E,r) data to the sixth-order polynomial

$$E(r) = a_0 + a_2(r - r_e)^2 + a_3(r - r_e)^3 + a_4(r - r_e)^4 + a_5(r - r_e)^5 + a_6(r - r_e)^6, \quad (4)$$

which has seven parameters. The reason that we use such an extensive function is that it is able to capture accurately the curvature of the PE function in the vicinity of the minimum and thus yield accurate values of the desired molecular constants. The first parameter, a_0, sets the energy at the minimum of the function, where $r = r_e$. The second-order constant, a_2, accounts for the harmonic (parabolic) character of the PE function, and the remaining constants describe the anharmonic quality of the potential. As we will see in Step 4, the molecular constants can be extracted from these constants.

Fit your CBS scan energies to equation (4). You will probably need initial guess values of the parameters. You can easily estimate a_0 and r_e from the position of

increasing quantum number is described by the anharmonicity constant $\tilde{\nu}_e\chi_e$. It can be calculated from your fit through

$$\tilde{\nu}_e\chi_e = \frac{B_e}{8}\left[15\left(1 + \frac{\alpha_e\tilde{\nu}_e}{6B_e^2}\right)^2 - \frac{12a_4r_e^2}{a_2}\right]. \quad (9)$$

Tabulate your molecular constants and compare them with the values reported in Herzberg.[3]

Questions and Further Thoughts

1. If you were going to obtain the molecular constants for DCl ($^2H^{35}Cl$), explain why you would not have to repeat the ab initio calculations (or even the polynomial fit). How, then, would you proceed to obtain the results?

2. A mathematical function that qualitatively describes real diatomic potential curves is the Morse potential,

$$E(r) = D_e\{1 - \exp[-\beta(r - r_e)]\}^2 + C, \quad (10)$$

where D_e is the dissociation energy, β is a constant that determines the curvature, r_e is the position of the minimum, as before, and C is the energy at the potential minimum (see Figure 1). Fit your ab initio data to a Morse potential. You can use the r_e value you read from your potential curve for an initial guess. D_e gives the strength of the molecular bond; since your data cover only a relatively small region near the bottom of the well, a reasonable initial guess for D_e is two times the range of energies you obtained in your scan. The Morse function indicates that β must have units of inverse length; $1/\beta$ is the characteristic length over which the potential energy curve "leans over" and begins to approach its asymptote, so 1 $Å^{-1}$ is a reasonable initial guess for β. $C + D_e$ is the energy of the separated H and Cl atoms; for the calculation you have done, -460 hartrees is a workable guess for C. Compare the fitted values of r_e and D_e with those in the literature,[2,3] and comment. Does your estimate of D_e, in particular, agree well? What would you have to do to get a better computational estimate?

3. What is the uncertainty in your value of the harmonic frequency, $\tilde{\nu}_e$? Use the standard deviation of a_2—see the *Model* sheet from your regression analysis.

4. If you want to calculate the molecular constants for an uncommon molecule, try something like $^2H^3H$ or $^3H^3H$.

5. The ionization energy of the helium cation (a one-electron atom) can be calculated exactly from the Schrödinger equation. Its value is -2 hartrees.[6] Determine this value from a CCSD/CBS calculation of He^+ (charge 1, multiplicity 2) and your CCSD/CBS energy of the neutral atom. See processes (1), (3a), and (3b). Compare your result with the experimental value.

Notes

1. See I. N. Levine, *Quantum Chemistry,* 5th ed., pp. 568–573, Prentice Hall (Upper Saddle River, NJ), 2000.
2. I. N. Levine, op cit., p. 492.
3. http://physics.nist.gov/PhysRefData/Compositions/
4. G. Herzberg, *Spectra of Diatomic Molecules,* 2nd ed., pp. 66–82, 90–97, 103–115, Van Nostrand Reinhold (New York), 1950.
5. G. Herzberg, op. cit., p. 534; see also http://webbook.nist.gov/chemistry and enter the formula for HCl. Check the box for Other Data—Constants of Diatomic Molecules. Scroll to the bottom of the table where the data for the ground state ($X\ ^1\Sigma^+$) are listed.
6. See P. Atkins and J. De Paula, *Physical Chemistry,* 8th ed., pp. 320–328, W. H. Freeman (New York), 2002.

increasing quantum number is described by the anharmonicity constant $\tilde{\nu}_e\chi_e$. It can be calculated from your fit through

$$\tilde{\nu}_e\chi_e = \frac{B_e}{8}\left[15\left(1 + \frac{\alpha_e\tilde{\nu}_e}{6B_e^2}\right)^2 - \frac{12a_4r_e^2}{a_2}\right]. \quad (9)$$

Tabulate your molecular constants and compare them with the values reported in Herzberg.[3]

Questions and Further Thoughts

1. If you were going to obtain the molecular constants for DCl ($^2H^{35}Cl$), explain why you would not have to repeat the ab initio calculations (or even the polynomial fit). How, then, would you proceed to obtain the results?

2. A mathematical function that qualitatively describes real diatomic potential curves is the Morse potential,

$$E(r) = D_e\{1 - \exp[-\beta(r - r_e)]\}^2 + C, \quad (10)$$

where D_e is the dissociation energy, β is a constant that determines the curvature, r_e is the position of the minimum, as before, and C is the energy at the potential minimum (see Figure 1). Fit your ab initio data to a Morse potential. You can use the r_e value you read from your potential curve for an initial guess. D_e gives the strength of the molecular bond; since your data cover only a relatively small region near the bottom of the well, a reasonable initial guess for D_e is two times the range of energies you obtained in your scan. The Morse function indicates that β must have units of inverse length; 1/β is the characteristic length over which the potential energy curve "leans over" and begins to approach its asymptote, so 1 $Å^{-1}$ is a reasonable initial guess for β. $C + D_e$ is the energy of the separated H and Cl atoms; for the calculation you have done, −460 hartrees is a workable guess for C. Compare the fitted values of r_e and D_e with those in the literature,[2,3] and comment. Does your estimate of D_e, in particular, agree well? What would you have to do to get a better computational estimate?

3. What is the uncertainty in your value of the harmonic frequency, $\tilde{\nu}_e$? Use the standard deviation of a_2—see the *Model* sheet from your regression analysis.

4. If you want to calculate the molecular constants for an uncommon molecule, try something like $^2H^3H$ or $^3H^3H$.

5. The ionization energy of the helium cation (a one-electron atom) can be calculated exactly from the Schrödinger equation. Its value is −2 hartrees.[6] Determine this value from a CCSD/CBS calculation of He^+ (charge 1, multiplicity 2) and your CCSD/CBS energy of the neutral atom. See processes (1), (3a), and (3b). Compare your result with the experimental value.

Notes

1. See I. N. Levine, *Quantum Chemistry*, 5th ed., pp. 568–573, Prentice Hall (Upper Saddle River, NJ), 2000.
2. I. N. Levine, op cit., p. 492.
3. http://physics.nist.gov/PhysRefData/Compositions/
4. G. Herzberg, *Spectra of Diatomic Molecules*, 2nd ed., pp. 66–82, 90–97, 103–115, Van Nostrand Reinhold (New York), 1950.
5. G. Herzberg, op. cit., p. 534; see also http://webbook.nist.gov/chemistry and enter the formula for HCl. Check the box for Other Data—Constants of Diatomic Molecules. Scroll to the bottom of the table where the data for the ground state ($X\ ^1\Sigma^+$) are listed.
6. See P. Atkins and J. De Paula, *Physical Chemistry*, 8th ed., pp. 320–328, W. H. Freeman (New York), 2002.

increasing quantum number is described by the anharmonicity constant $\tilde{\nu}_e\chi_e$. It can be calculated from your fit through

$$\tilde{\nu}_e\chi_e = \frac{B_e}{8}\left[15\left(1 + \frac{\alpha_e\tilde{\nu}_e}{6B_e^2}\right)^2 - \frac{12a_4r_e^2}{a_2}\right]. \qquad (9)$$

Tabulate your molecular constants and compare them with the values reported in Herzberg.[3]

Questions and Further Thoughts

1. If you were going to obtain the molecular constants for DCl ($^2H^{35}Cl$), explain why you would not have to repeat the ab initio calculations (or even the polynomial fit). How, then, would you proceed to obtain the results?

2. A mathematical function that qualitatively describes real diatomic potential curves is the Morse potential,

$$E(r) = D_e\{1 - \exp[-\beta(r - r_e)]\}^2 + C, \qquad (10)$$

where D_e is the dissociation energy, β is a constant that determines the curvature, r_e is the position of the minimum, as before, and C is the energy at the potential minimum (see Figure 1). Fit your ab initio data to a Morse potential. You can use the r_e value you read from your potential curve for an initial guess. D_e gives the strength of the molecular bond; since your data cover only a relatively small region near the bottom of the well, a reasonable initial guess for D_e is two times the range of energies you obtained in your scan. The Morse function indicates that β must have units of inverse length; 1/β is the characteristic length over which the potential energy curve "leans over" and begins to approach its asymptote, so 1 $Å^{-1}$ is a reasonable initial guess for β. $C + D_e$ is the energy of the separated H and Cl atoms; for the calculation you have done, −460 hartrees is a workable guess for C. Compare the fitted values of r_e and D_e with those in the literature,[2,3] and comment. Does your estimate of D_e, in particular, agree well? What would you have to do to get a better computational estimate?

3. What is the uncertainty in your value of the harmonic frequency, $\tilde{\nu}_e$? Use the standard deviation of a_2—see the *Model* sheet from your regression analysis.

4. If you want to calculate the molecular constants for an uncommon molecule, try something like $^2H^3H$ or $^3H^3H$.

5. The ionization energy of the helium cation (a one-electron atom) can be calculated exactly from the Schrödinger equation. Its value is −2 hartrees.[6] Determine this value from a CCSD/CBS calculation of He^+ (charge 1, multiplicity 2) and your CCSD/CBS energy of the neutral atom. See processes (1), (3a), and (3b). Compare your result with the experimental value.

Notes

1. See I. N. Levine, *Quantum Chemistry*, 5th ed., pp. 568–573, Prentice Hall (Upper Saddle River, NJ), 2000.
2. I. N. Levine, op cit., p. 492.
3. http://physics.nist.gov/PhysRefData/Compositions/
4. G. Herzberg, *Spectra of Diatomic Molecules*, 2nd ed., pp. 66–82, 90–97, 103–115, Van Nostrand Reinhold (New York), 1950.
5. G. Herzberg, op. cit., p. 534; see also http://webbook.nist.gov/chemistry and enter the formula for HCl. Check the box for Other Data—Constants of Diatomic Molecules. Scroll to the bottom of the table where the data for the ground state ($X\ ^1\Sigma^+$) are listed.
6. See P. Atkins and J. De Paula, *Physical Chemistry*, 8th ed., pp. 320–328, W. H. Freeman (New York), 2002.

APPENDIX C

Thermodynamic Quantities for Selected Substances at 298.15 K (25°C)

Substance	ΔH_f° (kJ/mol)	ΔG_f° (kJ/mol)	S° (J/mol-K)
Aluminum			
$Al(s)$	0	0	28.32
$AlCl_3(s)$	−705.6	−630.0	109.3
$Al_2O_3(s)$	−1669.8	−1576.5	51.00
Barium			
$Ba(s)$	0	0	63.2
$BaCO_3(s)$	−1216.3	−1137.6	112.1
$BaO(s)$	−553.5	−525.1	70.42
Beryllium			
$Be(s)$	0	0	9.44
$BeO(s)$	−608.4	−579.1	13.77
$Be(OH)_2(s)$	−905.8	−817.9	50.21
Bromine			
$Br(g)$	111.8	82.38	174.9
$Br^-(aq)$	−120.9	−102.8	80.71
$Br_2(g)$	30.71	3.14	245.3
$Br_2(l)$	0	0	152.3
$HBr(g)$	−36.23	−53.22	198.49
Calcium			
$Ca(g)$	179.3	145.5	154.8
$Ca(s)$	0	0	41.4
$CaCO_3$ (s, calcite)	−1207.1	−1128.76	92.88
$CaCl_2(s)$	−795.8	−748.1	104.6
$CaF_2(s)$	−1219.6	−1167.3	68.87
$CaO(s)$	−635.5	−604.17	39.75
$Ca(OH)_2(s)$	−986.2	−898.5	83.4
$CaSO_4(s)$	−1434.0	−1321.8	106.7
Carbon			
$C(g)$	718.4	672.9	158.0
$C(s$, diamond)	1.88	2.84	2.43
$C(s$, graphite)	0	0	5.69
$CCl_4(g)$	−106.7	−64.0	309.4
$CCl_4(l)$	−139.3	−68.6	214.4
$CF_4(g)$	−679.9	−635.1	262.3
$CH_4(g)$	−74.8	−50.8	186.3
$C_2H_2(g)$	226.77	209.2	200.8
$C_2H_4(g)$	52.30	68.11	219.4
$C_2H_6(g)$	−84.68	−32.89	229.5
$C_3H_8(g)$	−103.85	−23.47	269.9
$C_4H_{10}(g)$	−124.73	−15.71	310.0
$C_4H_{10}(l)$	−147.6	−15.0	231.0
$C_6H_6(g)$	82.9	129.7	269.2
$C_6H_6(l)$	49.0	124.5	172.8
$CH_3OH(g)$	−201.2	−161.9	237.6
$CH_3OH(l)$	−238.6	−166.23	126.8
$C_2H_5OH(g)$	−235.1	−168.5	282.7
$C_2H_5OH(l)$	−277.7	−174.76	160.7
$C_6H_{12}O_6(s)$	−1273.02	−910.4	212.1
$CO(g)$	−110.5	−137.2	197.9
$CO_2(g)$	−393.5	−394.4	213.6
$HC_2H_3O_2(l)$	−487.0	−392.4	159.8
Cesium			
$Cs(g)$	76.50	49.53	175.6
$Cs(l)$	2.09	0.03	92.07
$Cs(s)$	0	0	85.15
$CsCl(s)$	−442.8	−414.4	101.2
Chlorine			
$Cl(g)$	121.7	105.7	165.2
$Cl^-(aq)$	−167.2	−131.2	56.5
$Cl_2(g)$	0	0	222.96
$HCl(aq)$	−167.2	−131.2	56.5
$HCl(g)$	−92.30	−95.27	186.69
Chromium			
$Cr(g)$	397.5	352.6	174.2
$Cr(s)$	0	0	23.6
$Cr_2O_3(s)$	−1139.7	−1058.1	81.2
Cobalt			
$Co(g)$	439	393	179
$Co(s)$	0	0	28.4
Copper			
$Cu(g)$	338.4	298.6	166.3
$Cu(s)$	0	0	33.30
$CuCl_2(s)$	−205.9	−161.7	108.1
$CuO(s)$	−156.1	−128.3	42.59
$Cu_2O(s)$	−170.7	−147.9	92.36

Substance	ΔH_f° (kJ/mol)	ΔG_f° (kJ/mol)	S° (J/mol-K)
Fluorine			
$F(g)$	80.0	61.9	158.7
$F^-(aq)$	−332.6	−278.8	−13.8
$F_2(g)$	0	0	202.7
$HF(g)$	−268.61	−270.70	173.51
Hydrogen			
$H(g)$	217.94	203.26	114.60
$H^+(aq)$	0	0	0
$H^+(g)$	1536.2	1517.0	108.9
$H_2(g)$	0	0	130.58
Iodine			
$I(g)$	106.60	70.16	180.66
$I^-(aq)$	−55.19	−51.57	111.3
$I_2(g)$	62.25	19.37	260.57
$I_2(s)$	0	0	116.73
$HI(g)$	25.94	1.30	206.3
Iron			
$Fe(g)$	415.5	369.8	180.5
$Fe(s)$	0	0	27.15
$Fe^{2+}(aq)$	−87.86	−84.93	113.4
$Fe^{3+}(aq)$	−47.69	−10.54	293.3
$FeCl_2(s)$	−341.8	−302.3	117.9
$FeCl_3(s)$	−400	−334	142.3
$FeO(s)$	−271.9	−255.2	60.75
$Fe_2O_3(s)$	−822.16	−740.98	89.96
$Fe_3O_4(s)$	−1117.1	−1014.2	146.4
$FeS_2(s)$	−171.5	−160.1	52.92
Lead			
$Pb(s)$	0	0	68.85
$PbBr_2(s)$	−277.4	−260.7	161
$PbCO_3(s)$	−699.1	−625.5	131.0
$Pb(NO_3)_2(aq)$	−421.3	−246.9	303.3
$Pb(NO_3)_2(s)$	−451.9	—	—
$PbO(s)$	−217.3	−187.9	68.70
Lithium			
$Li(g)$	159.3	126.6	138.8
$Li(s)$	0	0	29.09
$Li^+(aq)$	−278.5	−273.4	12.2
$Li^+(g)$	685.7	648.5	133.0
$LiCl(s)$	−408.3	−384.0	59.30
Magnesium			
$Mg(g)$	147.1	112.5	148.6
$Mg(s)$	0	0	32.51
$MgCl_2(s)$	−641.6	−592.1	89.6
$MgO(s)$	−601.8	−569.6	26.8
$Mg(OH)_2(s)$	−924.7	−833.7	63.24
Manganese			
$Mn(g)$	280.7	238.5	173.6
$Mn(s)$	0	0	32.0
$MnO(s)$	−385.2	−362.9	59.7
$MnO_2(s)$	−519.6	−464.8	53.14
$MnO_4^-(aq)$	−541.4	−447.2	191.2
Mercury			
$Hg(g)$	60.83	31.76	174.89
$Hg(l)$	0	0	77.40
$HgCl_2(s)$	−230.1	−184.0	144.5
$Hg_2Cl_2(s)$	−264.9	−210.5	192.5
Nickel			
$Ni(g)$	429.7	384.5	182.1
$Ni(s)$	0	0	29.9
$NiCl_2(s)$	−305.3	−259.0	97.65
$NiO(s)$	−239.7	−211.7	37.99
Nitrogen			
$N(g)$	472.7	455.5	153.3
$N_2(g)$	0	0	191.50
$NH_3(aq)$	−80.29	−26.50	111.3
$NH_3(g)$	−46.19	−16.66	192.5
$NH_4^+(aq)$	−132.5	−79.31	113.4
$N_2H_4(g)$	95.40	159.4	238.5
$NH_4CN(s)$	0.0	—	—
$NH_4Cl(s)$	−314.4	−203.0	94.6
$NH_4NO_3(s)$	−365.6	−184.0	151
$NO(g)$	90.37	86.71	210.62
$NO_2(g)$	33.84	51.84	240.45
$N_2O(g)$	81.6	103.59	220.0
$N_2O_4(g)$	9.66	98.28	304.3
$NOCl(g)$	52.6	66.3	264
$HNO_3(aq)$	−206.6	−110.5	146
$HNO_3(g)$	−134.3	−73.94	266.4
Oxygen			
$O(g)$	247.5	230.1	161.0
$O_2(g)$	0	0	205.0
$O_3(g)$	142.3	163.4	237.6
$OH^-(aq)$	−230.0	−157.3	−10.7
$H_2O(g)$	−241.82	−228.57	188.83
$H_2O(l)$	−285.83	−237.13	69.91
$H_2O_2(g)$	−136.10	−105.48	232.9
$H_2O_2(l)$	−187.8	−120.4	109.6
Phosphorus			
$P(g)$	316.4	280.0	163.2
$P_2(g)$	144.3	103.7	218.1
$P_4(g)$	58.9	24.4	280
P_4(s, red)	−17.46	−12.03	22.85
P_4(s, white)	0	0	41.08
$PCl_3(g)$	−288.07	−269.6	311.7
$PCl_3(l)$	−319.6	−272.4	217
$PF_5(g)$	−1594.4	−1520.7	300.8
$PH_3(g)$	5.4	13.4	210.2
$P_4O_6(s)$	−1640.1	—	—
$P_4O_{10}(s)$	−2940.1	−2675.2	228.9
$POCl_3(g)$	−542.2	−502.5	325
$POCl_3(l)$	−597.0	−520.9	222
$H_3PO_4(aq)$	−1288.3	−1142.6	158.2

Substance	ΔH_f° (kJ/mol)	ΔG_f° (kJ/mol)	S° (J/mol-K)
Potassium			
$K(g)$	89.99	61.17	160.2
$K(s)$	0	0	64.67
$KCl(s)$	−435.9	−408.3	82.7
$KClO_3(s)$	−391.2	−289.9	143.0
$KClO_3(aq)$	−349.5	−284.9	265.7
$K_2CO_3(s)$	−1150.18	−1064.58	155.44
$KNO_3(s)$	−492.70	−393.13	132.9
$K_2O(s)$	−363.2	−322.1	94.14
$KO_2(s)$	−284.5	−240.6	122.5
$K_2O_2(s)$	−495.8	−429.8	113.0
$KOH(s)$	−424.7	−378.9	78.91
$KOH(aq)$	−482.4	−440.5	91.6
Rubidium			
$Rb(g)$	85.8	55.8	170.0
$Rb(s)$	0	0	76.78
$RbCl(s)$	−430.5	−412.0	92
$RbClO_3(s)$	−392.4	−292.0	152
Scandium			
$Sc(g)$	377.8	336.1	174.7
$Sc(s)$	0	0	34.6
Selenium			
$H_2Se(g)$	29.7	15.9	219.0
Silicon			
$Si(g)$	368.2	323.9	167.8
$Si(s)$	0	0	18.7
$SiC(s)$	−73.22	−70.85	16.61
$SiCl_4(l)$	−640.1	−572.8	239.3
$SiO_2(s,$ quartz)	−910.9	−856.5	41.84
Silver			
$Ag(s)$	0	0	42.55
$Ag^+(aq)$	105.90	77.11	73.93
$AgCl(s)$	−127.0	−109.70	96.11
$Ag_2O(s)$	−31.05	−11.20	121.3
$AgNO_3(s)$	−124.4	−33.41	140.9
Sodium			
$Na(g)$	107.7	77.3	153.7
$Na(s)$	0	0	51.45
$Na^+(aq)$	−240.1	−261.9	59.0
$Na^+(g)$	609.3	574.3	148.0
$NaBr(aq)$	−360.6	−364.7	141.00
$NaBr(s)$	−361.4	−349.3	86.82
$Na_2CO_3(s)$	−1130.9	−1047.7	136.0
$NaCl(aq)$	−407.1	−393.0	115.5
$NaCl(g)$	−181.4	−201.3	229.8
$NaCl(s)$	−410.9	−384.0	72.33
$NaHCO_3(s)$	−947.7	−851.8	102.1
$NaNO_3(aq)$	−446.2	−372.4	207
$NaNO_3(s)$	−467.9	−367.0	116.5
$NaOH(aq)$	−469.6	−419.2	49.8
$NaOH(s)$	−425.6	−379.5	64.46
Strontium			
$SrO(s)$	−592.0	−561.9	54.9
$Sr(g)$	164.4	110.0	164.6
Sulfur			
$S(s,$ rhombic)	0	0	31.88
$S_8(g)$	102.3	49.7	430.9
$SO_2(g)$	−296.9	−300.4	248.5
$SO_3(g)$	−395.2	−370.4	256.2
$SO_4^{2-}(aq)$	−909.3	−744.5	20.1
$SOCl_2(l)$	−245.6	—	—
$H_2S(g)$	−20.17	−33.01	205.6
$H_2SO_4(aq)$	−909.3	−744.5	20.1
$H_2SO_4(l)$	−814.0	−689.9	156.1
Titanium			
$Ti(g)$	468	422	180.3
$Ti(s)$	0	0	30.76
$TiCl_4(g)$	−763.2	−726.8	354.9
$TiCl_4(l)$	−804.2	−728.1	221.9
$TiO_2(s)$	−944.7	−889.4	50.29
Vanadium			
$V(g)$	514.2	453.1	182.2
$V(s)$	0	0	28.9
Zinc			
$Zn(g)$	130.7	95.2	160.9
$Zn(s)$	0	0	41.63
$ZnCl_2(s)$	−415.1	−369.4	111.5
$ZnO(s)$	−348.0	−318.2	43.9